UNIVERSITY OF OKLAHOMA

GRADUATE COLLEGE

EVALUATING THE IMPACTS OF STORM-SCALE AND ENVIRONMENTAL FACTORS ON STRATOSPHERE-TROPOSPHERE EXCHANGE ASSOCIATED WITH MIDLATITUDE CONVECTION

A THESIS

SUBMITTED TO THE GRADUATE FACULTY

in partial fulfillment of the requirements for the

Degree of

MASTER OF SCIENCE

By

Cole Shepherd
Norman, Oklahoma
2025

EVALUATING THE IMPACTS OF STORM-SCALE AND ENVIRONMENTAL FACTORS ON STRATOSPHERE-TROPOSPHERE EXCHANGE ASSOCIATED WITH MIDLATITUDE CONVECTION

A THESIS APPROVED FOR THE
SCHOOL OF METEOROLOGY

BY THE COMMITTEE CONSISTING OF

Dr. Cameron Homeyer (Chair)

Dr. Steven Cavallo

Dr. Elinor Martin

Acknowledgments

First and foremost, I thank my advisor, Dr. Cameron Homeyer for his support throughout my time in graduate school. He is a brilliant scientist and an exemplary advisor, and this work would have been impossible without his guidance and expertise. I came into graduate school with very little coding experience, and Dr. Homeyer invested many hours into developing my coding skills and assisting me when problems arose or when I was uncertain about how to perform a certain operation, despite having many other responsibilities as director of the school. I also learned a great deal about the upper troposphere and lower stratosphere as well as storm dynamics from Dr. Homeyer. He pushed me to think about many different facets and implications of my data, and I learned how to critically evaluate prior research in my field. Most of all, Dr. Homeyer was consistently positive, encouraging and supportive of my needs. I could not have asked for a better advisor and mentor in graduate school.

Next, I thank the entire Dynamics and Chemistry of the Summer Stratosphere (DCOTSS) field campaign science team for successfully orchestrating numerous flights and gathering the unprecedented dataset discussed and utilized in this study. This study and the entire field campaign were supported by the National Aeronautics and Space Administration (NASA) under Earth Venture Suborbital-3 program awards for DCOTSS (80NSSC19K0347, 80NSSC19K0326). I must also thank my committee members Dr. Steven Cavallo and Dr. Elinor Martin for enthusiastically agreeing to review and discuss my research. They attended my seminar and thesis defense, providing valuable feedback and asking thought-provoking questions. I also learned a great deal in the courses that they taught. Finally, I would like to acknowledge my research group members Hannah Fagan and Andrea Gordon. They provided support with coding and figure-making, and I frequently exchanged ideas with them.

Table of Contents

List of Tables

List of Figures

Abstract

Stratosphere-troposphere exchange (STE) plays a crucial role in Earth's climate; however, the significance of small-scale processes such as deep midlatitude convection to global STE remains understudied relative to large-scale processes. Tropopause-overshooting convection in the extratropics is especially important for stratospheric water vapor because the radiative forcing sensitivity of water vapor is greatest there. Thus, it is essential to understand what factors influence the strength and prevalence of overshooting storms and associated STE. The U.S. Dynamics and Chemistry of the Summer Stratosphere (DCOTSS) field campaign during 2021 and 2022 was the first large-scale airborne project for which sampling stratospheric impacts from overshooting convection was a primary focus. Our research utilizes the extensive DCOTSS dataset in combination with radar, satellite, and environmental observations to investigate the relationships between observed lower stratosphere composition change and various storm and environmental characteristics. We use back trajectories to link aircraft observations to observed storms and environments. Our results demonstrate greater magnitudes of troposphere-to-stratosphere transport for above-anvil cirrus plume (AACP)-producing storms and mesoscale convective systems (MCSs). In addition, the most extreme enhancements in water vapor and other tropospheric gases occur where the tropopause height is low and the depth of overshooting is high, especially for AACP-producing storms. These results provide new insights into types of storms and environments that generate the greatest stratopsheric impact. We also investigate the impact of storm and environmental characteristics on pathways for hydration (air mass transport and mixing versus ice sublimation), finding that they also modulate the frequencies of each process at different altitudes. Namely, mixing is found to be most prevalent in AACP-producing storms and MCSs, which can help explain transport differences between water vapor and other gases.

Chapter 1

Introduction

1.1 Stratosphere -troposphere exchange overview

Stratosphere-troposphere exchange (STE) plays a crucial role in Earth's climate and atmospheric chemistry. Because the tropopause is a stable layer, mixing across it is limited; however, there are several important mechanisms through which STE can occur and thus alter upper troposphere and lower stratosphere (UTLS) composition (Holton et al. 1995). The troposphere typically features high water vapor (H_2O) and low ozone (O_3) concentrations, while the opposite is true for the stratosphere. H_2O is a powerful greenhouse gas, and H_2O increases in the lower stratosphere facilitated by troposphere-to-stratosphere transport (TST) can result in significant UTLS cooling and surface warming (de F. Forster and Shine 1999; Solomon et al. 2010). Concurrently, increases in stratospheric aerosols from TST can have the opposite impact (Ban-Weiss et al. 2012). TST can also deliver other tropospheric chemicals and pollutants to the stratosphere, potentially altering O_3 chemistry. Meanwhile, stratosphere-to-troposphere transport (STT) increases O_3 in the troposphere which also increases surface radiative forcing (Holton et al. 1995; Tang et al. 2011; Phoenix and Homeyer 2021). The main mechanisms for STE include the Brewer-Dobson circulation (Brewer 1949; Dobson 1956; Butchart 2014), tropopause folding (Sprenger et al. 2003), Rossby wave breaking and isentropic transport (Pan et al. 2009), extratropical cyclones (Stohl 2001; Wernli and Bourqui 2002), tropical cyclones (Venkat Ratnam et al. 2016; Romps and Kuang 2009; Zhan and Wang 2012), and deep convection (Homeyer et al. 2014b; Smith et al. 2017).

In order to understand the role of various STE processes, subregions of the UTLS are typically defined and considered. The tropopause varies in height globally, decreasing from the equator to the poles, with a prominent discontinuity in height across the subtropical jet

(Holton et al. 1995). Isentropes above the 380K level reside exclusively in the stratosphere, a layer known as the stratospheric "overworld". Isentropes between 310 K and 380 K typically reside in the troposphere in the tropics and in the stratosphere in the extratropics, and this region is known as the "middleworld" (Hoskins 1991). Figure 1 from Hoskins (1991) provides a useful schematic illustrating these different layers. The portion of the middleworld that lies in the stratosphere and exists only in the extratropics is also known as the lowermost stratosphere, or LMS (Holton et al. 1995).

1.2 TST via overshooting convection

The most rapid source for STE is deep convection that overshoots the tropopause (hereafter, overshooting convection). Exchange between the overshooting top and the surrounding stratosphere can occur via turbulent mixing, facilitated by gravity wave breaking and Kelvin-Helmholtz instabilities (Wang 2003; O'Neill et al. 2021; Gordon and Homeyer 2022; Khordakova et al. 2022). Mixing with warmer stratospheric air along the edge of the overshooting top increases the temperature of the overshoot, thereby decreasing the negative buoyancy of these parcels and allowing some convectively lofted air to irreversibly detrain into the stratosphere (Wang 2003; Khordakova et al. 2022). Adiabatic transport of this detrained air and its constituent chemical species within the stratosphere can subsequently occur (Wang 2003; Ray et al. 2004).

While overshooting convection has long been recognized as a mechanism for STE in the tropics where convection is most abundant (Kley et al. 1982; Holton et al. 1995; Khaykin et al. 2009), the importance of overshooting convection to STE in midlatitudes has only gained widespread appreciation in recent decades. In particular, a number of research flights in the UTLS began to document fortuitous evidence of significant composition change associated with midlatitude overshooting storms (e.g. Poulida et al. 1996; Fischer et al. 2003; Hegglin et al. 2004; Ray et al. 2004; Homeyer et al. 2014b) and studies of remote sensing data revealed surprisingly large frequencies of overshooting and its impacts (Cooney et al. 2018; Jensen et al. 2020; Liu et al. 2020; Tinney and Homeyer 2021). H_2O enhancements above background levels, O_3 reductions, and enhancements of other tropospheric trace gases and pollutants such as carbon monoxide (CO) in the stratosphere have all been observed (Poulida et al. 1996; Fischer et al. 2003; Ray et al. 2004; Khordakova et al. 2022). In fact, TST associated with midlatitude convection is now recognized to be more frequent and reach deeper into the stratosphere than that for tropical convection (Jensen et al. 2020; Liu et al. 2020). In addition, both observations and model simulations have demonstrated substantial STT associated with overshooting convection (e.g. Poulida et al. 1996; Pan et al. 2014; Gordon and Homeyer 2022; Auth and Homeyer 2023).

Overshooting convection is uniquely important to UTLS chemistry. Namely, unlike other mechanisms of uplift, convection can rapidly transport boundary layer air upward with limited dilution (Fischer et al. 2003; Ray et al. 2004; Mullendore et al. 2005; Homeyer et al. 2014b). For example, species with short lifetimes in the boundary layer, such as nitrogen oxides (NOx), sulfur dioxide (SO_2), volatile organic compounds, and halogen compounds, can enter the stratosphere, where their lifetimes increase such that they modify local chemistry and aerosol behavior (Dickerson et al. 1987; Poulida et al. 1996; Ray et al. 2004; Mullendore et al. 2005; Randel et al. 2010; Homeyer et al. 2014b; Gordon et al. 2024). If storms occur near fossil fuel or biomass burning emissions sources, TST of pollutants such as CO and NOx can occur (Fromm and Servranckx 2003; Jost et al. 2004; Duncan et al. 2007; Park et al. 2009; Randel et al. 2010; Ban-Weiss et al. 2012). Meanwhile, downward transport of stratospheric air near overshoots and around storm anvils can deliver O_3 and other stratospherically abundant trace gases to the upper troposphere (Poulida et al. 1996; Tang et al. 2011; Pan et al. 2014; Gordon and Homeyer 2022; Auth and Homeyer 2023). Convection has been found to be a substantial source of tropospheric O_3 in the midlatitude spring and summer, which has implications for surface climate (Tang et al. 2011; Phoenix and Homeyer 2021).

Overshooting convection can generate significant stratospheric hydration, far exceeding that possible in most large-scale processes. Large quantities of ice crystals can be detrained from the overshooting cloud into the lower stratosphere, bypassing the freeze drying that occurs in the Brewer-Dobson circulation (BDC) within the tropics (Grosvenor et al. 2007; Weinstock et al. 2007; Khaykin et al. 2009). Any injected ice crystals are typically small, so their fall rates are slow, and they can quickly sublimate into the dry and comparatively warm stratosphere (Wang 2003; Grosvenor et al. 2007; Corti et al. 2008; de Reus et al. 2009; Le and Gallus Jr. 2012). Thus, H_2O delivery to the LS can occur via both air mass transport & mixing and ice sublimation (Homeyer et al. 2024), leading to strong H_2O enhancements, as demonstrated in both observations (Hegglin et al. 2004; Ray et al. 2004; Hanisco et al. 2007; Corti et al. 2008; de Reus et al. 2009; Khaykin et al. 2009; Homeyer et al. 2014b; Herman et al. 2017; Smith et al. 2017; Khordakova et al. 2022; Homeyer et al. 2023) and modeling studies (Wang 2003; Chaboureau et al. 2007; Grosvenor et al. 2007; Chemel et al. 2009; Le and Gallus Jr. 2012; Dauhut et al. 2018; Homeyer et al. 2014a). These studies also repeatedly demonstrate that enhancements in H_2O within the stratosphere reach higher altitudes than passive, boundary layer tracers (Phoenix and Homeyer 2021; Tinney and Homeyer 2021; Gordon and Homeyer 2022; Gordon et al. 2024). Moreover, unlike alternative large-scale mechanisms in the extratropics, TST associated with overshoots can frequently reach into the overworld (Cooney et al. 2018; Homeyer et al. 2023), leading to substantial hydration in this region. Weinstock et al. (2007) found a convective contribution of 0.7% to air mass between the 380 K and 390 K isentropes associated with summertime convection over North America in a limited region; however, the percentage of H_2O in this layer due to convection was much higher, generally ranging from 10% to 35%. Other studies have also demonstrated a strong convective contribution to LS water vapor on a large scale (Dessler and Sherwood 2004; Hanisco et al. 2007; Tinney and Homeyer 2021).

1.3 Extratropical overshooting convection and the DCOTSS field campaign

A major reason why extratropical convection was not considered important to global STE until recently was a belief that the impacts of midlatitude overshoots were limited to the LMS. Because large-scale sinking motion occurs in the extratropical stratosphere associated with the BDC, chemicals lofted into the LMS can only remain in the stratosphere for a short time – a few months at most (Dessler and Sherwood 2004). For this reason, it was assumed there was no mechanism for tropospheric air to reach the overworld outside of the tropics (Stohl et al. 2003). Recent analyses of extratropical overshooting convection have shattered this paradigm, demonstrating that storms frequently reach well into the overworld, leading to significant H_2O enhancements above 380 K (Homeyer et al. 2014b; Herman et al. 2017; Smith et al. 2017; Cooney et al. 2018; Khaykin et al. 2022; Homeyer et al. 2023). Although it remains true that overshooting volume decreases exponentially with height above the tropopause and that the majority of overshooting material does remain in the LMS (Weinstock et al. 2007; Solomon et al. 2016; Smith et al. 2017), midlatitude overshooting convection is responsible for a significant portion of the H_2O observed in the overworld near regions of frequent convection (Hanisco et al. 2007; Weinstock et al. 2007; Smith et al. 2017; Khaykin et al. 2022; Homeyer et al. 2024). In fact, extratropical convection has greater stratospheric hydration potential than tropical convection due to differences in UTLS thermodynamics. Namely, H_2O enhancements from overshoots are constrained by saturation mixing ratios. Since isentropes in the lower stratosphere are warmer at higher latitudes, a single event can result in much greater hydration compared to an equivalent storm in the tropics (Dessler and Sherwood 2004; Tinney and Homeyer 2021). Furthermore, the tropopause is lower, so deeper overshooting is more common despite lower numbers of storms overall (Liu et al. 2020).

North America has been identified as a global hotspot for overshooting storms during the spring and summer. It experiences the largest and deepest convectively driven LS hydration on the globe (Randel et al. 2012; Schwartz et al. 2013; Anderson et al. 2017; Jensen et al. 2020). A strong maximum in overshooting convection occurs over the U.S. Great Plains, with a weaker secondary maximum in the southeastern U.S. (Cooney et al. 2018; Liu et al. 2020). Using satellite observations, Tinney and Homeyer (2021) found that this convection regionally leads to a 100% increase in LS H_2O, a 50% increase in LS CO, and a 40% decrease in LS O_3 within 3 days of overshooting. When accumulating overshooting effects during long simulations, convection has been found to be responsible for as much as a 20% increase in LMS water vapor during the springtime and a 7–11% increase during summertime over the central and eastern U.S. (Phoenix and Homeyer 2021). More broadly, Dessler and Sherwood (2004) and Sayres et al. (2024) found the contribution over North America seasonally to be as high as 40%. The existence of the North American monsoon anticyclone (NAMA)—a large circulation that dominates UTLS flow over the U.S. during the summer—magnifies the stratospheric impacts of storms by increasing the residence time of convectively impacted air in the lower stratosphere over the CONUS and increasing the probability of this air reaching the overworld via lofting induced by diabatic heating above 360 K (Chang et al. 2023). Chang et al. (2023) estimated that 45% of air transported above the tropopause via convection within the NAMA remains in the stratosphere after 30 days, and the fraction of such air that reaches the tropical LS can be as high as 9% in July. As a result, convection can increase lower stratospheric H_2O over the U.S. by 1 ppm during the warm season (Phoenix and Homeyer 2021; Sayres et al. 2024). Thus, convective TST over the U.S. is uniquely important to the stratospheric composition at-large.

Because extratropical convection strongly influences lower stratospheric composition, improving our understanding of TST associated with storms in the midlatitudes, and especially the critically important North American region, is important. Most of the initial in situ observations of midlatitude overshooting convection discussed previously (e.g. Jost et al. 2004; Ray et al. 2004) were incidental. While other prior work has sought to tackle the problem of convective STE via model simulations (e.g. Wang 2003; Mullendore et al. 2005; Grosvenor et al. 2007; Gordon and Homeyer 2022), these simulations typically focus on individual storms and do not provide a sense of the global impacts of midlatitude convection on stratospheric composition. Broader efforts to characterize convective influence using satellite data (e.g. Tinney and Homeyer 2021) have been valuable, but the relatively low resolution of such data relative to convective processes and influence under-represents the true magnitude of convective perturbations (Anderson et al. 2017; Jensen et al. 2020). Although some field campaigns, such as the Deep Convective Clouds and Chemistry experiment (DC3; Barth et al. 2015) and the NASA Studies of Emissions and Atmospheric Composition Clouds and Climate Coupling by regional surveys campaign (Toon et al. 2016, SEAC^{4}RS;), did include a few flights that explicitly targeted stratospheric air impacted by convection over the U.S. (Homeyer et al. 2014b; Herman et al. 2017; Smith et al. 2017), overshooting convection was not the sole focus of these campaigns. The 2021-2022 Dynamics and Chemistry of the Summer Stratosphere (DCOTSS) field campaign over the U.S. was the first large-scale field campaign for which gathering in situ measurements of stratospheric air impacted by convection was the explicit goal. DCOTSS included 22 flights that measured stratospheric composition post-convection, resulting in 20 times more sampling of convective H_2O enhancements in the stratosphere than all prior studies (Homeyer et al. 2023). This novel dataset is thus vital to improving our knowledge of STE associated with overshooting convection in extratropical environments over North America.

DCOTSS data can also be used to further our understanding of the conditions that determine the abundance, longevity, and depth of overshooting storms and associated stratospheric impact, which is the primary focus of this study. As the climate warms, midlatitude Convective Available Potential Energy (CAPE) is projected to increase, which could increase the frequency of overshooting convection; however, tropopause heights are also likely to increase (Stohl et al. 2003) which could mitigate this effect. At the same time, there is evidence suggesting that stability in the LMS will decrease as the climate warms (Stohl et al. 2003), which would heighten overshoot depth. Taking these competing influences into account, Tinney et al. (2024) found using simulations of convection that overshooting frequency and depth are indeed projected to increase in a warming climate. Given the strong radiative impacts of stratospheric H_2O enhancements in the LMS, which experiences the greatest hydration from overshooting storms, this could engender a positive feedback that enhances climate warming (Solomon et al. 2010; Dessler et al. 2013, 2016; Banerjee et al. 2019). Extratropical overshooting convection will hence play a key role in the stratospheric H_2O feedback.

Aside from impacts on surface radiative forcing, increases in lower stratospheric H_2O would also cause LS cooling, which can induce upward and poleward shifts in the subtropical and eddy-driven jets, as well as a strengthening of the BDC. These changes can also affect circulation patterns closer to the surface, generating substantial alterations in regional climate (Butchart 2014; Charlesworth et al. 2023). Furthermore, increased overshooting convection may lead to an increase in O_3-destroying radicals in the lower stratosphere if stratospheric temperatures are sufficiently low (Anderson et al. 2012, 2017). For all of these reasons, understanding how different atmospheric conditions will affect the magnitude and depth of convective hydration is of critical importance.

1.4 Impact of storm and environmental character-istics on TST

Although projected thermodynamic changes suggest future increases in overshooting convection and stratospheric hydration, we do not yet fully understand the influence of environmental and storm-scale properties on the frequency, depth, or volume of overshoot material. No prior studies have comprehensively interrogated this issue using in situ observations. Model simulations and satellite observations have illuminated some connections between these storm attributes and overshooting characteristics, but understanding remains limited. For instance, previous modeling work established that stratospheric H_2O and CO impacts from midlatitude convection are greater in environments with lower tropopause heights Phoenix and Homeyer (2021); Tinney and Homeyer (2021). UTLS and overshoot temperature have also been noted as a potential constraint on H_2O enhancements Gordon et al. (2024); Homeyer et al. (2024); Phoenix and Homeyer (2021). While warmer tropopause temperatures can facilitate increased hydration due to lesser saturation constraints Tinney and Homeyer (2021), the existence of increased CO in lower tropopause environments indicates that stronger transport is also occurring Phoenix and Homeyer (2021). When comparing different storm modes, modeling work has suggested that overshooting and associated transport is strongest and reaches the highest altitudes in discrete storms (Mullendore et al. 2005, 2013; Bigelbach et al. 2014), but more abundant TST occurs during Mesoscale Convective Systems (MCSs) due the scale of the storm system and frequency of weaker overshoots (Bigelbach et al. 2014). Accordingly, greater UTLS enhancements in boundary layer tracers have been found for MCSs versus other convective modes (Poulida et al. 1996; Le and Gallus Jr. 2012; Homeyer et al. 2014b); however, these comparisons involved singular events.

Other studies have examined the impacts of storms which produce above-anvil cirrus plumes (AACPs) on STE. AACPs are associated with particularly intense storms and an increased risk of severe weather (Bedka et al. 2015; Homeyer et al. 2017; Bedka et al. 2018). AACPs form when strong storm-relative winds in the UTLS lead to especially strong and sustained gravity breaking near the overshooting cloud top (Wang 2003; Homeyer et al. 2017; O'Neill et al. 2021; Gordon and Homeyer 2022). The vigorous gravity wave breaking on the downstream side of the overshooting top generates a hydraulic jump, which drives longer-lived and deeper transport above the equilibrium level, producing a plume of water vapor and ice 1–4 km above the anvil (Homeyer et al. 2017; O'Neill et al. 2021; Murillo and Homeyer 2022; Gordon and Homeyer 2022). Model simulations have suggested that storms with AACPs (hereafter "AACP storms") exhibit a greater magnitude and depth of TST (Homeyer et al. 2017; O'Neill et al. 2021; Gordon and Homeyer 2022), but only one observational case study has confirmed this result (Gordon et al. 2024). Interestingly, Gordon et al. (2024) observed extreme tracer enhancements specifically within cloud material (anvil and AACP), which was not the case for H_2O. This could indicate that AACP presence may be a crucial factor in determining whether significant transport of boundary layer chemicals into the stratosphere occurs. Furthermore, all of the AACP storm modeling work highlighted has consisted of idealized supercells, which are typically characterized by having the strongest updrafts of convective storms (Gordon and Homeyer 2022; O'Neill et al. 2021; Wang 2003). We do not know if these patterns will hold true for weaker AACP-producing convection, such as non-supercellular discrete cells or clusters. Moreover, modeling studies have rendered conflicting results with regard to whether or not AACP formation leads to greater H_2O enhancements in the LMS given thermodynamic controls (Homeyer et al. 2017; O'Neill et al. 2021; Gordon and Homeyer 2022). Thus, a major goal of this study is to evaluate whether the same TST characteristics will emerge when examining a much larger and more diverse set of storms.

Additional work has examined the importance of air mass transport and mixing versus ice sublimation to stratospheric hydration associated with overshooting storms. While most earlier studies focused on ice injection and sublimation as the primary pathway for stratospheric hydration from overshooting convection (e.g. Grosvenor et al. 2007; Corti et al. 2008; de Reus et al. 2009; Khaykin et al. 2009; Dessler et al. 2016; Herman et al. 2017; Smith et al. 2017), recent studies have demonstrated a large contribution from air mass transport and mixing as well (Homeyer et al. 2014b, 2024). An initial survey of H_2O enhancements sampled during DCOTSS revealed that only $\approx$50% of all measured stratospheric hydration resulted from ice sublimation, while the remainder resulted from air mass transport (Homeyer et al. 2024); however, Homeyer et al. (2024) did not consider how different storm and environmental conditions might influence which transport pathway dominates. In this study, we explore which conditions favor ice sublimation versus air transport & mixing as the primary source of stratospheric H_2O enhancement.

1.5 Study overview and goals

This study seeks to investigate the connection between different storm attributes, such as storm mode, AACP presence, overshoot depth, and environmental characteristics such as tropopause height and temperature, and the magnitude and depth of convection-driven stratospheric composition change measured during DCOTSS. Based on prior work, we hypothesize that AACPs and lower tropopause heights foster greater TST in overshooting storms, but the impacts of other variables are less clear. We also explore the impact of storm and environmental characteristics on the dominant pathway of H_2O delivery to the stratosphere. Analyzing different storm and environmental variables and how they influence TST utilizing a large observational dataset allows us to confirm hypotheses and settle disagreements raised in prior case studies and model simulations, enhancing our understanding of which conditions promote the largest convection-driven stratospheric composition changes. This can add nuance to our understanding of convective contributions to stratospheric composition in the midlatitudes. To accomplish this work, we link each observation of overshoot material to its storm of origin. Storm and environmental attributes are then examined using radar, satellite, and environmental data. All of the variables examined are listed in Table 2.1. The trace gases analyzed include H_2O, CO, and O_3. Although changes in stratospheric CO resulting from convection do not substantially impact stratospheric chemistry (Mullendore et al. 2005), CO was chosen for analysis because it serves as an effective boundary layer tracer (Dickerson et al. 1987; Mullendore et al. 2005). Unlike H_2O, CO is passive and thus unaffected by phase changes or saturation constraints (Mullendore et al. 2005).

Chapter 2

Data & Methods

2.1 Aircraft measurements

The DCOTSS field campaign was based primarily in Salina, Kansas and utilized the NASA high-altitude ER-2 aircraft with 12 onboard instruments to sample the meteorological characteristics and chemical composition of the lower stratosphere post-convection. Figure 1 in Homeyer et al. (2024) shows a map of all flight paths. The maximum altitude reached was 21.25 km. 29 flights occurred during July-August 2021 and May-July 2022. All aircraft data examined in this study are sourced from the airborne collection of the DCOTSS archive (NASA/LARC/SD/ASDC 2022). We use measurements of H_2O, O_3, and CO to identify and characterize convective TST. H_2O is measured using the Harvard Herriott Hygrometer (HHH)—a tunable diode laser direct absorption instrument—within the Harvard Water Vapor instrument (HWV), providing H_2O mixing ratio measurements at 1-second intervals. Its precision is 0.1 ppmv and its accuracy is 5–10% (Sargent et al. 2013). HWV also contains the Harvard Lyman-α photo-fragment fluorescence instrument (LyA), which has an accuracy of 10% and precision of 6% (Weinstock et al. 1994). During one flight (24 June 2022), HHH failed, so LyA measurements are used instead. Sargent et al. (2013) demonstrates good agreement between the two instruments despite the lower precision of LyA. Measurements of altitude (accuracy of 15 m), pressure (accuracy $\pm$ 0.5 hPa), air temperature (accuracy $\pm$ 0.3 K) and potential temperature (accuracy ranges from $\pm$ 0.5 K at 200 hPa to $\pm$ 1.5 K at 50 hPa) are recorded at 1-second intervals by the meteorological measurement system (MMS; Scott et al. 1990). O_3 mixing ratios are measured at 1-s intervals by the Rapid Ozone Experiment (ROZE) instrument, with an accuracy of 6% and a precision of $\pm$ 1 ppbv in the stratosphere (Hannun et al. 2020). Finally, measurements of CO are provided by the Harvard University Picarro Cavity Ringdown Spectrometer (HUPCRS), which is a modified G2401-m Picarro gas analyzer that completes samples at 2.2-second intervals (Crosson 2008). HUPCRS observations are averaged to 10-second intervals for analysis. HUPCRS CO measurements have an accuracy of $\pm$ 3.5 ppbv and a precision of 2.8 ppbv.

2.2 Reanalysis data and tropopause diagnosis

Hourly assimilations from the fifth generation of European Center for Medium Range Weather Forecasts reanalysis (ERA5) are utilized to diagnose environmental characteristics in the vicinity of the aircraft observations as well as the overshooting storms that occurred during DCOTSS. ERA5 provides output from 1940–Present at a horizontal grid spacing of 31 km and at 137 pressure levels from the surface to 0.1 hPa (Hersbach et al. 2020). However, our analysis utilizes ERA5 output on a 0.25° latitude-longitude grid and 37 unevenly spaced model levels. Tropopause altitudes in the ERA5 analyses are identified using the lapse rate tropopause definition (Meteorology 1957), for which each ERA5 profile is interpolated to a regular 100-m grid using cubic splines prior to application, yielding an uncertainty in tropopause altitude of $\leq$500 m (Hoffmann and Spang 2022; Tinney et al. 2022). We note that ERA5 tropopause heights are not expected to capture distortions in tropopause altitude by the storms themselves, which is a potential source of error in our diagnosis of matched storm attributes such as overshooting depth. Convection can increase tropopause height by as much as 1.5 km (Homeyer et al. 2014b,a). Tropopause identification can also fail in double tropopause environments, which has been noted to result in up to 20% missed overshoot identifications in prior studies (e.g. Solomon et al. 2016). It is unclear to what extent this is a problem in the DCOTSS dataset, but the likely outcome would simply be data excluded from our analysis. ERA-5 wind fields were also used for trajectory calculations and storm matching as described in Section 2.5.

2.3 Radar data and overshoot definition

Gridded NEXRAD WSR-88D radar (GridRad) data from DCOTSS (NASA/LARC/SD /ASDC 2022) provide merged volumes of all NOAA NEXRAD radar observations over the contiguous U.S. spanning 24–50°N latitude and 235–294°E longitude with ≈0.02° (≈2 km) horizontal grid spacing at 10-minute intervals and corresponding overshoot identifications. Vertical grid spacing of GridRad volumes is 0.5 km from 0.5–7 km above mean sea level and 1 km thereafter up to 22 km above mean sea level (Homeyer and Bowman 2022). Radar reflectivity data are quality-controlled to remove non-meteorological echoes and other artifacts, following recommendations in Homeyer and Bowman (2022). GridRad overshoot identifications for DCOTSS are based on 10-dBZ echo top heights, ERA5 tropopause altitudes, and tropopause-level reflectivity. Echo top height is defined as the highest level within each convective radar column at which reflectivity exceeds 10 dBZ so long as the two vertical levels below this height have valid echoes ≥10 dBZ. The resulting echo top heights have an uncertainty of ± 1 km. ERA5 tropopause characteristics are then interpolated to the echo top locations on the grid for overshoot identification. If a column has echo top heights exceeding the ERA-5 tropopause altitude, it is classified as overshooting convection so long as the tropopause-level reflectivity is ≥20 dBZ.

2.4 Satellite data

Geostationary Observing Earth Satellite (GOES) imagery over North America for DCOTSS (NASA/LARC/SD /ASDC 2022) provide visible and longwave infrared (IR) cloud-top imagery, including the minimum IR brightness temperature of overshooting storms. GOES data are analyzed at the same 10-minute time intervals of the GridRad data and have 2-km resolution. Although IR brightness temperatures are generally a good proxy for cloud top temperature and heights (Bedka et al. 2015), we note that minimum brightness temperatures reached by the overshoots tend to be colder when the tropopause is higher and colder

(Solomon et al. 2016), so brightness temperature is not a perfect proxy for overshoot altitude or depth. In addition, brightness temperatures can be affected by the characteristics of the surrounding environment via mixing (Adler and Mack 1986; Setvák et al. 2010).

2.5 Convective feature identification and storm ma-tching

For the aircraft observations, we utilize a record of "convective feature" identifications based on subjectively-identified H_2O enhancements above the prevailing stratospheric background concentration and coincident with GridRad- and GOES-sourced overshoot trajectories within the prior 5-day period, as introduced in Homeyer et al. (2023) and discussed further in Homeyer et al. (2024), to initially isolate convective observations for analysis. The DCOTSS dataset consists of 28.4 hours of convective feature sampling in total (Homeyer et al. 2023).

To examine the storm-scale and environmental characteristics that create the observed stratospheric composition changes, we then link each convective feature in the aircraft data back to its likely source storm. Specifically, ERA5 data are used to generate five-day isentropic back trajectories with position information at 10-minute intervals, initialized every second along the flight path. At each 10-minute timestep of the trajectory calculation, the distance between the particle location and each overshooting pixel in the GridRad domain is calculated. A storm is identified as a match if it contains at least one overshooting pixel that falls within 100 km of the particle location so long as the angle between the wind vector and particle-to-pixel direction vector is less than $<90°$. The second criterion ensures that the particle location is downstream of the overshoot. A maximum of three overshoot matches along the back trajectory are allowed. We then impose a further constraint on distance: the maximum allowable distance increases from 0 to 100 km during the first 4 days at a rate of 25 km per day. In some cases, multiple overshooting regions satisfy these stricter match criteria; however, to compare individual storm attributes, it becomes necessary to narrow down each convective feature to one matched storm that was responsible for the majority of the observed perturbations. Hence, in these cases, the most recent match is chosen. A map of all matched storms is presented in Fig. 2.1. In total, 32,313 observations are successfully matched with storms, including 14,657 matched to AACP storms and 17,656 matched to non-AACP storms; and 12,330 matched to single cells, 7869 matched to multicells, and 12,114 matched to MCSs; however many one-second observations are linked to the same matched storm at the same timestep. If considering only unique matches, those counts are 1,465, 623, 843, 546, 367, and 556 respectively.

Once a single matched storm (overshooting region) is identified, GridRad, GOES, and ERA5 data from the time and location of the match are used to characterize the attributes of the storm and its environment. A full list of all the flight data and matched storm data variables analyzed is provided in Table 2.1.

2.6 Storm mode classification

Storm mode classification in this study applies an objective technique outlined in Murphy et al. (2023) with a few modifications. In particular, GridRad data are used to identify closed contours of column-maximum reflectivity $\geq$30 dBZ at each time. Reflectivity from non-convective events that exceed 30 dBZ is filtered out. The number of storms within each closed contour is then counted as the number of local echo top maxima based on the 10 dBZ threshold as described in Section 2.5. Multiple maxima that are less than 10 km apart are reduced such that only the highest-altitude maximum is retained. If a matched storm falls within one of these contours, the following criteria are used to classify the storm mode:

1. If the area of the contour is greater than 3000 km^2, and the maximum length scale of contour is at least 100 km, then the storm is classified as an MCS.

2. If the area of the contour is greater than 3000 km^2 but the maximum length scale is less than 100 km, then the storm is classified as multicellular.

3. If the area of the contour is less than 3000 km^2 and there are three or fewer echo top maxima in the contour, then the storm is classified as a single cell.

4. If the contour area is less than 3000 km^2 but there are more than three echo top maxima within the contour, then the storm is classified as multicellular.

3000 km^2 is an appropriate threshold delineating the area that a large single cell (i.e., a supercell) can reach (Homeyer et al. 2020). Two or three echo top maxima occurring within a small contour are classified as single cellular in an attempt to account for storms that have cyclic updraft generation such that multiple updrafts exist at once but do not persist as separate entities. The 100 km threshold for MCS classification is based on Houze Jr. (2004)'s definition of an MCS.

2.7 Above anvil cirrus plume identification

AACPs are identified manually using GOES images. Matched storms that occur during daytime are evaluated for AACP presence using sandwich imagery, in which semi-transparent visible images and IR images are superimposed. Nighttime AACPs are identified using IR images only. In visible satellite imagery, an AACP appears as a cloud mass emanating from near the overshooting top with a smoother texture than the underlying anvil. It also commonly casts a shadow on the anvil (Wang et al. 2011; Homeyer et al. 2017; Bedka et al. 2018; Murillo and Homeyer 2022). In IR satellite images, a stratospheric AACP materializes as an enclosed feature of relatively warm brightness temperature relative to the surrounding anvil emanating from near the overshooting top, which itself appears as a small, anomalously cold area (Bedka et al. 2015; Homeyer et al. 2017; Murillo and Homeyer 2022). Examples of plume identification are displayed in Fig. 2.2. While some convective storms have AACPs that are colder than the anvil, these plumes occur in the troposphere (Murillo and Homeyer 2022). Since this study focuses on the impacts of AACPs on stratospheric composition, cold AACPs are ignored in our analysis.

2.8 Determination of hydration processes

We investigate the relative contributions of air mass mixing and ice sublimation to observed stratospheric hydration in the DCOTSS data via O_3-H_2O and θ-H_2O correlations, where θ is potential temperature. Correlation analysis follows the technique used in Homeyer et al. (2024). For each constant-altitude flight observation within a convective feature, correlations are evaluated over a 21-s period centered on the observation time (Exception: the first and last 10 s of each convective feature are excluded, since a consecutive 21-s interval centered on the observation time is not available.). Pearson correlation coefficients (P) are calculated to determine linear correlations within each interval. P ranges from -1 (pure negative correlation) to 1 (pure positive correlation). Convective features that occurred during vertical profiles are also removed because correlations associated with typical strong UTLS gradients in O_3, H_2O and θ could influence the results in these cases. In total, 22.3 hours or 78% of convective feature observations were retained for tracer-tracer analysis.

We use the same thresholds as Homeyer et al. (2024) to define resulting O_3-H_2O correlations as positive, weak, or negative. Namely, if $P \geq 0.35$, O_3 and H_2O are considered positively correlated; if $P \leq -0.35$, O_3 and H_2O are negatively correlated, and if $-0.35 < P < 0.35$, O_3 and H_2O are weakly correlated. Meanwhile, a binary classification system is used for θ-H_2O correlations: θ and H_2O are negatively correlated if $P < 0$ and positively correlated if $P \geq 0$. These correlations are then used to determine the dominant hydration process for each H_2O enhancement. Weak O_3-H_2O correlation is associated with ice sublimation, while negative correlation is associated with air mass transport and mixing, as air with relatively high H_2O and low O_3 concentrations is deposited into the stratosphere. Positive O_3-H_2O correlations can be associated with either mixing or ice sublimation. In this case, θ-H_2O correlations are necessary for such classification. The two possible scenarios for positive O_3-H_2O correlations are:

1. Saturation-limited transport and mixing – If the overshoot is very cold, low saturation vapor pressure limits H_2O within the overshoot, while the surrounding stratosphere is hydrated via ice sublimation. This results in less H_2O and colder temperatures in the overshoot than the surrounding stratosphere, leading to positive O_3-H_2O and θ-H_2O correlations once air mass mixing occurs.

2. Ice sublimation with strong cooling – Ice sublimation can result in cooling, leading to descent of hydrated stratospheric air. As long as this hydrated air retains higher O_3 levels than the surrounding air at its new, lower altitude, O_3-H_2O correlation is positive, while θ-H_2O correlation is negative.

2.9 Data analysis

We utilize background-relative concentrations of trace gases to most accurately characterize the magnitude of stratospheric composition change. To transform all observations in our dataset to background-relative concentrations, we first bin DCOTSS flight observations of H_2O, CO, and O_3 according to the tropopause-relative altitude of the flight measurement calculated using the ERA5 tropopause. Bins range from -1 to 5 km at 0.5-km resolution. For all three trace gases, the background concentrations in each altitude bin are established by calculating the median value of all non-convective flight observations in that bin measured during the campaign. Each convectively-influenced measurement is then divided by the background concentration in its altitude bin to determine its background-relative concentration (ratio).

Once the flight observation is normalized to background-relative values, we investigate relationships between observed perturbations of H_2O, O_3, and CO and the different storm and environment variables. For the sake of brevity, we present only the most meaningful results (i.e. storm and environmental patterns that generate clear and noticeable patterns when plotted and are most useful to our understanding of TST), which are bolded in Table 2.1. Due to a lack of aged AACP storms and MCSs, we eliminate data from storms with an overshoot age of 72 hours or more when comparing the different storm categories, given that overshoot age had a significant impact on the magnitude of observed chemical perturbations (not shown). We also exclude storms that occurred where the tropopause exceeded 15.5 km owing to a lack of AACP storms at these tropopause heights. Two-sample Kolmogorov - Smirnov tests are used to determine whether different variables analyzed produce statistically significant effects.

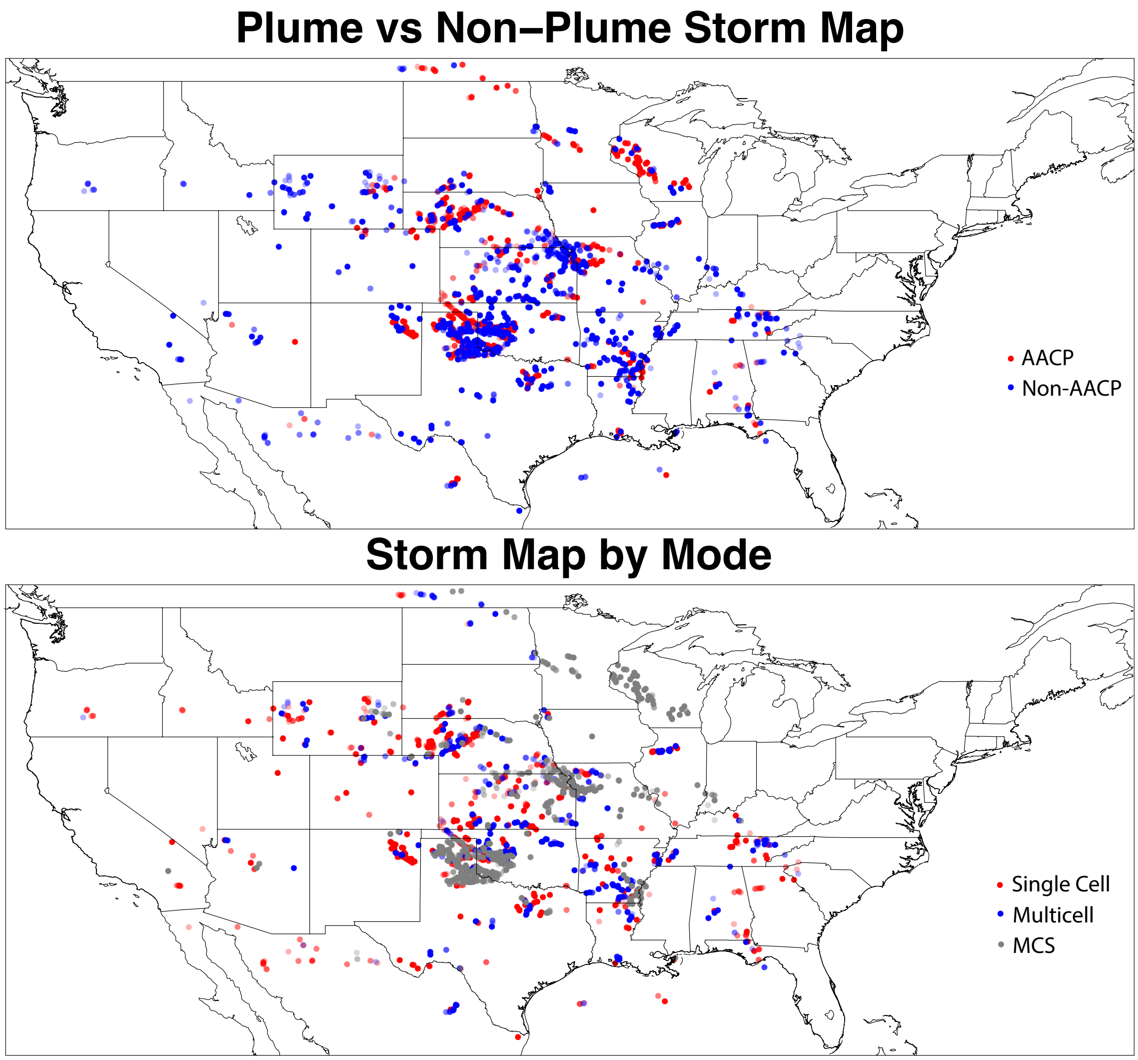

Figure 2.1: Maps of all trajectory-matched storms. The top panel displays the locations of AACP (red dots) and non-AACP storms (blue dots), and the bottom panel separates the storms by mode: single cell (red dots), multicell (blue dots), and mesoscale convective system (MCS; gray dots).

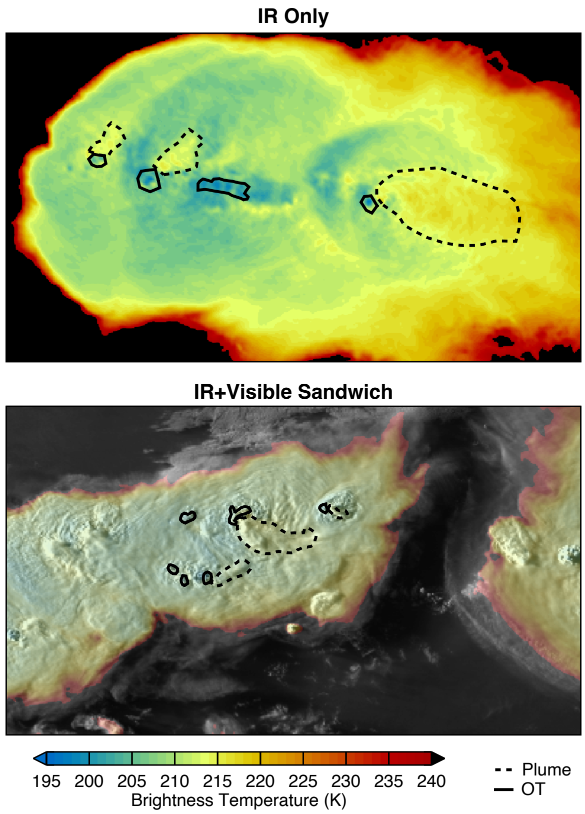

Figure 2.2: Examples of manual AACP identification using (top) infrared (IR) GOES imagery and (bottom) GOES IR+visible sandwich imagery. Dashed lines outline AACPs while solid lines outline overshooting tops.

Variable	All storms	Plume v Non-Plume	Mode
Tropopause-relative height of flight observation	**X**	**X**	**X**
Absolute observation height	X	X	
Absolute observation θ	X	X	
Median Storm Echo Top Height			
Maximum Storm Echo Top Height			
Median Storm Echo Top θ			
Maximum Storm Echo Top θ			
Median storm overshoot depth	X	X	X
Maximum storm overshoot depth	**X**	**X**	**X**
Tropopause height at storm location	**X**	**X**	**X**
Tropopause θ at storm location	X	X	
Tropopause temperature at storm location	X		X
Minimum brightness temperature of storm	**X**	**X**	
Median reflectivity of storm	X	X	
Maximum reflectivity of storm	X		X
Severe weather reports			
Time between overshoot and observation	X		

Table 2.1: All storm and environmental variables investigated in this study. Variables that produce meaningful patterns for all storms and/or easily apparent and statistically significant differences between AACP and non-AACP storms or among different storm modes when plotted are marked with an X. Plots are included and discussed in detail only for the results deemed most robust and useful, which are marked in bold.

Chapter 3

Results

3.1 Influence of AACP occurrence and storm mode on TST magnitude and depth

Figure 9 from Gordon et al. (2024) displays trace gas measurements in the DCOTSS dataset at relative altitude to the tropopause, demonstrating that H_2O enhancements reached higher than CO enhancements as found in prior modeling work (Phoenix and Homeyer 2021; Gordon and Homeyer 2022). To expand upon these summative DCOTSS results, we similarly evaluate trace gas enhancements partitioned into various subsamples of storms. The resulting profiles are displayed in Figs. 3.1 and 3.2. Results are only included for a particular altitude bin if at least 180 seconds of sampling within convective features occurred in that altitude bin for a particular storm category; however, CO measurements occurred over 10-second intervals, and our instruments did not always record a valid measurement every second for H_2O or O_3 either. Thus, actual sample sizes may be less than 180, especially for CO. H_2O sample sizes for each bin within the profiles are listed in Table 3.1.

When examining all storms, trace gas concentrations decrease with increasing tropopause-relative altitude; however, strong differences appear for H_2O versus CO. CO enhancements relative to background are weaker throughout the distribution and stronger enhancements ($> 1.5\times$ background) are restricted to lower altitudes, in agreement with prior DCOTSS analyses. Strong differences appear when examining AACP vs non-AACP storms—AACP storms produce greater H_2O enhancements at all levels but especially near the tropopause. This result validates the subset of prior modeling studies indicating greater H_2O transport in AACP storms. Storm mode differences in stratospheric hydration are minimal among all storms; however, Fig. 3.2 reveals that AACP storms produce different magnitudes of hydration for different storm modes. Most notably, AACPs have a significant impact on hydration in single-cell storms at all above-tropopause levels, with median H_2O values for AACP single cells clearly surpassing 75th percentile H_2O values for non-AACP single cells. Weaker differences exist between AACP and non-AACP storms of other modes, except in the first km above the tropopause for MCSs. AACP storms also produce greater CO enhancements, particularly in the first 2 km above the tropopause, and Fig. 3.2 demonstrates that single-cell storms are once again responsible for the majority of this difference. Unlike that for H_2O, a large spike in CO enhancement above the tropopause does not appear for AACP MCSs. Bedka et al. (2018) found that MCSs have shorter-lived AACPs compared to discrete storms, which could help explain the larger impact of AACP presence on CO enhancements from single-cell storms versus MCSs. Meanwhile, stronger hydration can still occur near the tropopause since H_2O reaches higher altitudes than CO. Although Bedka et al. (2018) did not consider multicells, it is also plausible that they would have similarly shorter-lived AACPs than single cells.

O_3 concentrations in our convective samples tend to exceed background levels in the upper troposphere and decline rapidly with altitude, such that O_3 is nearly uniformly below background levels at tropopause-relative altitudes >1 km. O_3 appears to rebound for some samples 3–4 km above tropopause. This pattern indicates the presence of both upward transport of O_3-poor tropospheric air and simultaneous downward transport and entrainment of O_3-rich stratospheric air (similar to that diagnosed in the model simulations of Gordon and Homeyer (2022)). Some of this downward transport appears to be entrained into the upper part of the overshooting top, while some reaches the upper troposphere. AACP storm samples exhibit greater O_3 below the tropopause and lesser O_3 above the tropopause than non-AACP samples, demonstrating stronger TST and STT in AACP storms. O_3 also rebounds less at higher levels in AACP storms, providing further evidence of deeper TST occurring in AACP storms. Once again, these AACP impacts are strongest in single-cell storms. While these explanations are plausible hypotheses to explain the observed patterns in O_3, minimal samples below the tropopause exist in our dataset, meaning that the indication of increased STT in AACP storms may not be a trustworthy result.

Evaluating storm mode differences separately from plume effects also unveils notable differences. Figure 3.2 reveals that MCSs produce greater hydration 0–1 km above the tropopause regardless of AACP presence. This is not the case for CO transport. Instead, when comparing among non-AACP storms, MCSs result in greater CO enhancements at higher levels ($\geq$ 2km relative altitude). Furthermore, MCSs exhibit less O_3 reduction than other modes at lower levels, but no rebound in O_3 at higher levels. This pattern appears in samples linked to both AACP and non-AACP storms, though the difference is more substantial for non-AACP storms. These results for CO and O_3 may suggest that non-AACP MCSs result in weaker transport just above the tropopause but are more efficient at lofting tropospheric air to higher levels compared to other non-AACP storms. This could result from more voluminous transport in MCSs, allowing a slight upward shift in the distribution of CO values at higher altitudes despite weaker dynamics and fewer extreme values. AACP presence then outweighs these mode differences, producing stronger transport near the tropopause among MCSs and greater transport to high levels for all modes. While these explanations are plausible, the CO results at higher altitudes may be an artifact of sample biases given very small sample sizes, especially for non-AACP storms. The O_3 pattern observed at high relative altitudes can also be explained by differences in overworld air entrainment. Non-AACP single cell and multicell samples exhibit a spike in O_3 concentrations at high altitudes, so perhaps non-AACP storms are drawing in more overworld air, but only so long as there is not too much storm clustering. MCSs perturb the atmosphere on a larger scale, so it may be difficult to entrain undisturbed overworld air.

Overall these results clearly demonstrate the unique capability of intense, discrete storms with AACPs to transport H_2O and other trace gases deep into the stratosphere. This agrees with results from Gordon and Homeyer (2022). Though not a focus of this study, we also find evidence of greater STT in single-cell AACP storms, which deviates from Gordon and Homeyer (2022)'s results. Finally, MCSs also have unique TST characteristics compared to other modes, depositing greater H_2O near the tropopause and creating greater O_3 reduction (and potentially greater CO enhancement) at higher tropopause-relative altitudes.

3.2 Influence of AACPs and storm mode on H_2O transport processes

Next, we evaluate air transport & mixing versus ice sublimation frequencies for H_2O enhancement as a function of tropopause-relative height (Figs. 3.3 and 3.4). Once again, results are only included for altitude bins where at least 180 seconds of convective feature sampling occurred. Actual sample sizes are slightly smaller than the total number of seconds of sampling since the first and last 10s of each convective feature are excluded as described in section 2.8. Overall, about equal frequencies of mixing versus sublimation were observed in our storm matching dataset, in alignment with Homeyer et al. (2024)'s results for all DCOTSS observations, though AACP storms and MCSs produced slightly higher mixing frequencies. When examining all storms (Fig. 3.3, top left), sublimation weakly dominates just below the tropopause, while mixing weakly dominates at most above-tropopause altitudes. The increase in mixing up to 3 km is a somewhat unexpected result, given the greater heights reached by H_2O versus other boundary layer trace gases is often attributed to ice sublimation processes. It is possible that ice sublimation did occur at higher levels but in some cases induced significant cooling, causing the hydrated air to subside before measurement—a process described in Homeyer et al. (2024). Ice crystals may also fall before sublimating completely. At 3–4 km, however, mixing dips again, which could indicate that the level of maximal air mass transport is being exceeded. Although mixing rebounds again at 4–5 km, the sample size is small. A major difference exists between AACP and non-AACP storms. Air transport & mixing frequencies increase with observation height among non-AACP storms before dipping at higher levels, exceeding sublimation frequencies only in a narrower range (1-3 km), whereas they uniformly exceed ice sublimation frequencies above the tropopause for AACP storms. At the highest altitudes, ice sublimation spikes sharply for non-AACP storms (possibly an artifact of sample bias). These results are consistent with the theory that AACPs drive deeper and longer-lived air mass transport into the stratosphere (Homeyer et al. 2017; O'Neill et al. 2021; Gordon and Homeyer 2022).

Figure 3.3 also displays differences in transport characteristics when examining different storm modes. Single cells and multicells follow the typical pattern of increasing mixing frequency with altitude, while mixing dominates at all altitudes for MCSs and especially so ($\sim$60%) at higher altitudes. The full breakdown into all six joint storm categories in Fig. 3.4 provides further clarity on these differences. First, non-AACP storms of all modes exhibit a reduction in mixing frequency at higher altitudes. Although mixing slightly dominates over sublimation at the highest level for non-AACP MCSs, the spread is much smaller than at lower altitudes. Conversely, AACP multicells and MCSs exhibit high ($\sim$70%) mixing frequency at altitudes $>$3 km above tropopause. Although AACP single cells do experience a spike in ice sublimation at higher altitudes, it is much smaller than that for non-AACP single cells, both of which may be impacted by sample biases. These results would suggest that AACPs drive deeper air mass transport for all storm modes; however, sample sizes at these high altitudes are relatively small. In addition, higher mixing frequency at high altitudes in non-AACP MCSs compared to other non-AACP storms may explain why CO was notably elevated in such samples, while H_2O was not.

3.3 Influence of tropopause height on observed TST

To explore environmental constraints on observed UTLS composition impacts from overshooting, we focus on a well-established one—tropopause height. If we explore tropopause heights among storm populations (Fig. 3.5), it becomes apparent that the distribution of tropopauses skews slightly lower for AACP storms compared to non-AACP storms, particularly for single-cell storms. Multicell storms do not show consistent differences between

AACP and non-AACP populations and occur most commonly in higher tropopause environments ($\geq$15 km). Examining tropopause height against overshoot depth reveals that maximum overshoot depths are reduced in high-tropopause environments (not shown). Together, this may explain the weaker impacts of AACP multicell storms (compared to other AACP storms) diagnosed previously. Namely, H_2O enhancements in our AACP multicell samples are more likely to be saturation limited and linked to overshoots that may have struggled to reach as deep into the stratosphere given the higher-tropopause environment. Conversely, lower tropopause heights likely contribute to exceptionally strong trace gas enhancements observed for AACP single cells.

To further examine how different tropopause heights impact TST, we now present a two-dimensional analysis of trace gas changes as a function of tropopause height in the matched storm environment and tropopause-relative altitude of the aircraft measurement (Figs. 3.6 – 3.8). Once again, results are only included if $>$ 180s of sampling occurred within a particular two-dimensional bin. Actual sample sizes for each trace gas are listed on the figures. It is clear that hydration peaks near the tropopause in low tropopause environments; however, hydration above 1.5 km tropopause-relative altitude is not substantially impacted by tropopause height (Fig. 3.6). The weaker hydration near the tropopause at high tropopause heights likely stems primarily from greater saturation constraints due to colder UTLS temperatures and secondarily from greater difficulty of deep overshooting and transport. Hydration at higher tropopause-relative altitude may be less affected by tropopause height because it is more dependent on ice sublimation. AACP impacts also appear to be maximized near the tropopause in low tropopause environments. The contrast between AACP and non-AACP hydration then fades as tropopause height increases and saturation constraints become more limiting; however, some difference still remains, indicating that AACP vs. non-AACP differences discussed in 3.1 cannot be entirely from varying tropopause heights among samples. Storm mode comparison reveals that single cells produce stronger enhancements at medium tropopause heights than other modes, including at mid and upper levels. Partitioning the 2-D analysis by both AACP presence and storm mode (Fig. 3.9), reveals that AACP storms drive this difference. Meanwhile, MCSs produce the strongest hydration at higher tropopause heights. This may result from transport volume differences discussed previously. Our two dimensional analysis of CO change in Fig. 3.7 results in somewhat different patterns. As for H_2O, CO enhancements peak just above the tropopause, but overall CO enhancement maximizes at medium tropopause heights (13.5–15 km) rather than in the lowest tropopause height bin as for H_2O. AACP storms also produce the strongest enhancements in CO compared to non-AACP storms at medium tropopause heights. MCSs are an exception, with CO enhancements maximizing at the highest tropopause altitudes. Otherwise, storm mode differences generally mirror those for H_2O. Medium tropopause environments likely produce the strongest overshooting storms, as they provide a balance between largest instability and a low enough tropopause, resulting in maximum CO transport, while saturation limits likely constrain H_2O more in these environments. A more intriguing difference for CO compared to H_2O is a weak decrease in concentration at greater tropopause-relative altitudes and within medium-high tropopause environments, which likely indicates downward transport. Although these differences are not statistically significant in all cases, O_3 analysis affirms the results.

Two-dimensional analysis of O_3 observations in Fig. 3.8 provides further insight into the impact of storm characteristics on both upward and downward transport in the UTLS. In low tropopause environments, O_3 declines from slightly above background concentrations to well below background concentrations as tropopause-relative altitude increases. Meanwhile, at medium to high tropopause altitudes, O_3 is more uniform with tropopause-relative height, potentially indicating a lower depth of TST. At high altitudes within high-tropopause environments, O_3 is strongly enhanced for most storm categories. These results are statistically significant and mirror the CO reductions appearing at high altitudes in the same environments, indicating likely downward transport and entrainment of overworld air. As is true for CO, O_3 concentrations in MCSs are an exception, exhibiting strong reductions at high tropopause-relative altitudes even in high tropopause environments. These results suggest that strong TST becomes more difficult in high-tropopause environments and may be outweighed by downward transport.

Partitioning the 2-D analysis by both AACP presence and storm mode (Figs. 3.9, 3.10, and 3.11) further illuminates differences in transport characteristics among storm modes. Figure 3.9 confirms that AACP single cells drive the elevated hydration for single cells at medium tropopause heights, especially at mid and upper levels ($\geq$1.5 km above tropopause). The notion that the strongest overshooting updrafts occur at medium tropopause heights would explain this pattern, (i.e. strong transport counteracts increasing saturation limits) given that AACP single cells exhibit the strongest TST generally. Conversely, MCSs produce greater and deeper hydration in high tropopause environments regardless of AACP presence, indicating that the storm mode itself is the primary driver of this effect. Results for CO enhancement are similar, though less robust, with differences from H_2O paralleling the bulk analysis in Figs. 3.6 & 3.7. Because CO transport does not reach as high of levels as H_2O transport, it is even more severely limited in high-tropopause environments when considering single cells and multicells. O_3 analysis also reveals similar results, with AACP single cells inducing low O_3 compared to other categories in medium tropopause environments and both AACP and non-AACP MCSs generating relatively low O_3 in high tropopause environments (Fig. 3.11). O_3 enhancement in high tropopause environments is present for AACP single cells, non-AACP single cells, and non-AACP multicells, mirroring CO reductions. These outcomes further demonstrate that significant TST becomes more difficult in high-tropopause environments and downward transport may be more impactful, except for in MCSs.

Figures 3.12 and 3.13 show results of applying the 2-D analysis to diagnosed air transport & mixing and ice sublimation processes from H_2O-O_3 and H_2O-θ correlation. When considering all storms, frequencies display opposite relationships to the altitude of the

H_2O enhancements at low versus high storm tropopause heights. When the tropopause height is low, H_2O enhancements are increasingly sourced from transport and mixing as the height above the tropopause increases. Conversely, at high tropopause heights, H_2O near the tropopause is primarily sourced from mixing, while sublimation dominates at higher tropopause-relative altitudes, as implied by the trace gas results. At medium tropopause heights, there is no clear trend overall since different storm modes exhibit opposing trends. All panels in Figs. 3.12 and 3.13 demonstrate the same general pattern in high-tropopause environments, except for AACP MCSs, which exhibit strong mixing at high depths in high-tropopause environments and no decrease in CO with altitude (Fig. 3.10). On the other hand, the dominance of mixing at higher altitudes in lower tropopause environments appears to contradict the observed pattern of stronger H_2O versus CO enhancements at these altitudes (Figs. 3.6 and 3.7). A possible explanation is that stronger H_2O enhancement still occurs because ice sublimation is a more efficient hydration process—even a small amount of ice sublimation relative to mixing can lead to a large water vapor impact due to the high contrast in H_2O concentrations between the troposphere and stratosphere (Homeyer et al. 2024). Meanwhile, mixing may be increasingly saturated limited at these higher altitudes. The result may also simply be due to sample bias, as sample size is small in this bin.

3.4 Influence of overshoot depth on observed TST

In this section, we analyze the relationship between storm overshoot depth and stratospheric composition changes, comparing different storm populations. We first present a histogram displaying differences in storm-maximum overshoot depth (Fig. 3.14). AACP storms have greater maximum overshoot depth than non-AACP storms, in agreement with radar and satellite observations from Homeyer et al. (2017). The difference between AACP and non-AACP maximum overshoot depth is especially pronounced for single cells and nonexistent for multicells. These outcomes suggest AACP presence and overshoot depth are correlated, especially when considering single-cell storms, which could be a confounding variable that contributes to the large differences in H_2O and CO observed for AACP vs non-AACP storms discussed previously. Comparison of different storm modes also illustrates that MCSs have the greatest maximum overshoot depths in our sample, despite having slightly lower median overshoot depths because the areas of overshoot features are larger in MCSs (not shown).

To examine how storm overshoot depth modulates the magnitude and depth of stratospheric composition change, we once again employ two-dimensional analysis, this time as a function of overshoot depth rather than storm tropopause height. Figures 3.15 and 3.16 show that H_2O and CO enhancements in the first 1.5 km above tropopause increase strongly with increasing overshoot depth. At higher tropopause-relative altitudes, CO enhancements still increase weakly with overshoot depth while H_2O concentrations do not. These results suggest that overshoot depth impacts both the magnitude of TST and the depth of transport. The discrepancy between H_2O and CO relationships at higher tropopause-relative altitudes may stem from saturation constraints (which are likely most prevalent at higher altitudes in deeper overshoots). Figures 3.15 – 3.17 also highlight that AACP storms produce stronger and deeper perturbations in H_2O, CO, and O_3 at most overshoot depths compared to non-AACP storms, indicating that some portion of the AACP vs. non-AACP differences discussed in section 3.1 can be attributed to the AACPs themselves, rather than the greater overshoot depth of AACP storms. In addition, AACPs appear to make a larger difference in TST when overshoot depth is greater. Storm mode comparison reveals that MCSs exhibit the strongest increase in hydration with overshoot depth of any mode near the tropopause, whereas single cells are the only mode that exhibit an increase in hydration with overshoot depth at high tropopause-relative altitudes. CO sensitivities to storm mode are broadly similar, though less pronounced and maximized at low tropopause-relative altitudes in single cells and multicells. Meanwhile, O_3 (Fig. 3.17) exhibits no clear or consistent sensitivity to overshoot depth, likely due to the opposing effects of changes in upward and downward transport; however, a notable result appears among storms with low overshoot depth: O_3

is enhanced at higher tropopause-relative altitudes, consistent with weak CO reductions in these bins.

The strong trends in hydration with overshoot depth among MCSs may be related to overshoot abundance. Because median overshoot depth is lower overall in MCSs compared to other modes, LMS hydration may be more sensitive to overshoot depth (i.e. stronger storms are more necessary to release significant H_2O sufficiently above the tropopause that it remains in the stratosphere). This explanation relies on the assumption that MCSs with the highest maximum overshoot depth also have increased median overshoot depth, which we have confirmed for our samples (not shown). Thus, when MCSs contain stronger overshooting at-large, H_2O transported by abundant overshoots is more likely to be released substantially above the tropopause. Meanwhile, CO is more reliant on the strongest overshoots within the MCS to reach the stratosphere since it cannot be transported to as high of altitudes by a single updraft and is not saturation limited.

Examination of overshoot depth impacts for all six storm categories (Figs. 3.18 – 3.20) yields additional insights into the variation of transport characteristics among storm types. Hydration just above the tropopause increases strongly with overshoot depth for both types of MCSs, but the increase is especially pronounced for AACP MCSs. CO enhancements increase with overshoot depth regardless of observation altitude for both AACP single cells and AACP MCSs. H_2O and CO observations for non-AACP storms are generally more similar across modes and exhibit weaker trends. Patterns for O_3 were not particularly clear; however, one notable result is that the O_3 enhancements at higher altitudes are linked to AACP single cells and non-AACP single cells and multicells with low overshoot depth.

Plots of air transport & mixing frequency further elucidate the observed patterns of composition change (Figs. 3.21 and 3.22). At higher altitudes, mixing frequency increases considerably as overshoot depth increases. This pattern holds for both AACP and non-AACP storms, though AACP samples contain higher mixing frequencies regardless of storm overshoot depth, again consistent with the trace gas analyses. Meanwhile, at lower altitudes, air transport & mixing frequency decreases with increasing overshoot depth. Thus, the height of tropospheric air injection appears to increase as overshoot depth increases. Examining all storm categories reveals that single cells drive the increase in mixing with overshoot depth at high altitudes which is consistent with discrete cells having a more specific injection altitude. The trend is quite extreme: ice sublimation strongly dominates at low overshoot depths, while mixing strongly dominates at high overshoot depths. This is coincident with the diagnosed CO decreases and O_3 increases implying downward transport, indicating that entrainment of warmer, drier stratospheric air may be leading to a spike in ice sublimation under these conditions (Dauhut et al. 2018). It is unclear if non-AACP single cells follow this same pattern due to limited samples at high overshoot depth.

MCSs exhibit different patterns from other modes. Mixing dominates at both low and high altitudes when overshoot depth is < 4 km. An abundance of overshoots injecting material at various depths likely produces this lack of specificity in injection altitude. In addition, MCSs have greater mixing frequency than any mode when considering storms with low overshoot depths. The full breakdown showcases opposing trends for AACP MCSs versus non-AACP MCSs – mixing frequeuncy peaks at low overshoot depth among AACP MCSs, while non-AACP MCS exhibits sublimation dominance at low overshoot depth and mixing dominance at medium overshoot depth. The presence of mixing-induced H_2O enhancements at high tropopause-relative altitudes sourced from AACP MCSs with low maximum overshoot depth could indicate that lofting of MCS-injected air occurred, perhaps due to confinement within the NAMA circulation. It could also result from ERA-5 primary tropopause misdiagnoses in double tropopause environments.

Another notable difference among modes occurs at the highest overshoot depths: when overshoot depth is > 4 km, mixing frequency dips for MCSs. This may also explain the observed patterns in H_2O and CO enhancements for MCSs. A significant portion of the increased hydration observed near the tropopause at high overshoot depths must be due to sublimation, which explains why increases in CO with overshoot depth are less extreme than increases in H_2O. The reason for increased sublimation among H_2O enhancements in stronger MCSs may be tied to greater saturation constraints, as minimum brightness temperature measurements reveal that MCSs in our dataset are generally colder (not shown). Increased sublimation could also be a byproduct of stronger gravity wave breaking leading to increased entrainment of warmer and drier stratospheric air, as explained in Dauhut et al. (2018); however, our results for other storm modes somewhat contradict Dauhut et al. (2018)'s explanation for the relationship between hydration and overshoot depth, showcasing increased hydration and increased mixing when overshoots are deeper and a maximum in stratospheric entrainment at low overshoot depths. Dauhut et al. (2018) also does not consider AACP effects, which are greatest in single cell storms. Rather, Dauhut et al. (2018) simulations involved an MCS in a tropical environment, so perhaps their hypothesis is most useful under these conditions specifically. Nonetheless, our results do not necessarily disprove Dauhut et al. (2018)'s hypothesis among single cells and multicells, as it is still possible that the entrainment increases at greater overshoot depths but this is simply outweighed by stronger increases in transport and mixing, especially when AACPs are involved. In addition, the notion that low overshoot depth maximizes stratospheric entrainment is a somewhat perplexing result which cannot be easily explained. Perhaps it is a real effect. It is also possible that these low overshoot depths with high stratospheric air entrainment represent cases where the tropopause was misdiagnosed. Sample biases may also come into play, as injected air could be transported to very different environment between injection and measurement.

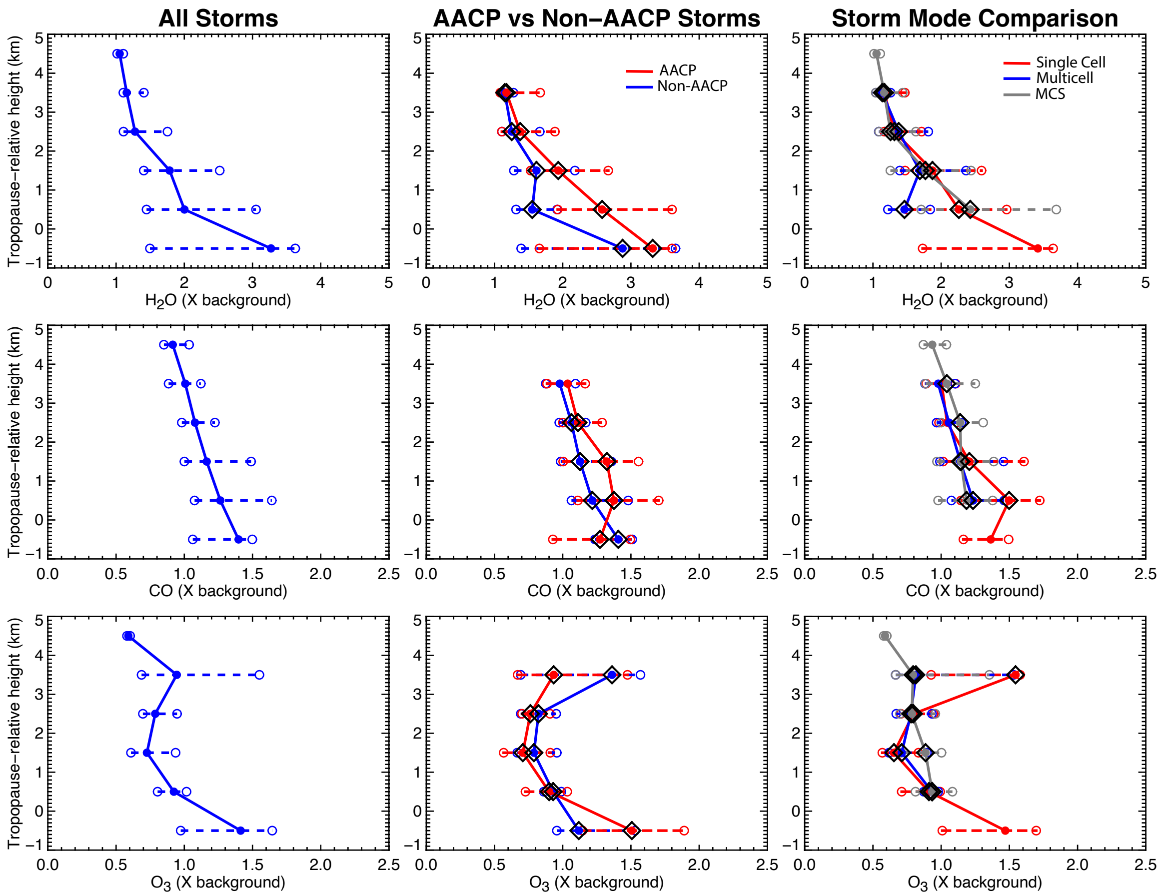

Figure 3.1: Background-relative concentrations of (top row) H_2O, (middle row) CO, and (bottom row) O_3 as a function of tropopause-relative height for (left-to-right) all storms, AACP vs. non-AACP storms, and storm modes. Solid circles denote median background-relative concentrations within each bin, while open circles denote 25th and 75th percentile background-relative concentrations. Black diamonds indicate statistically significant differences between AACP and non-AACP storms or between one storm mode and both other storm modes. For each bin, results are shown only if $\geq$180 s of convective feature sampling occurred.

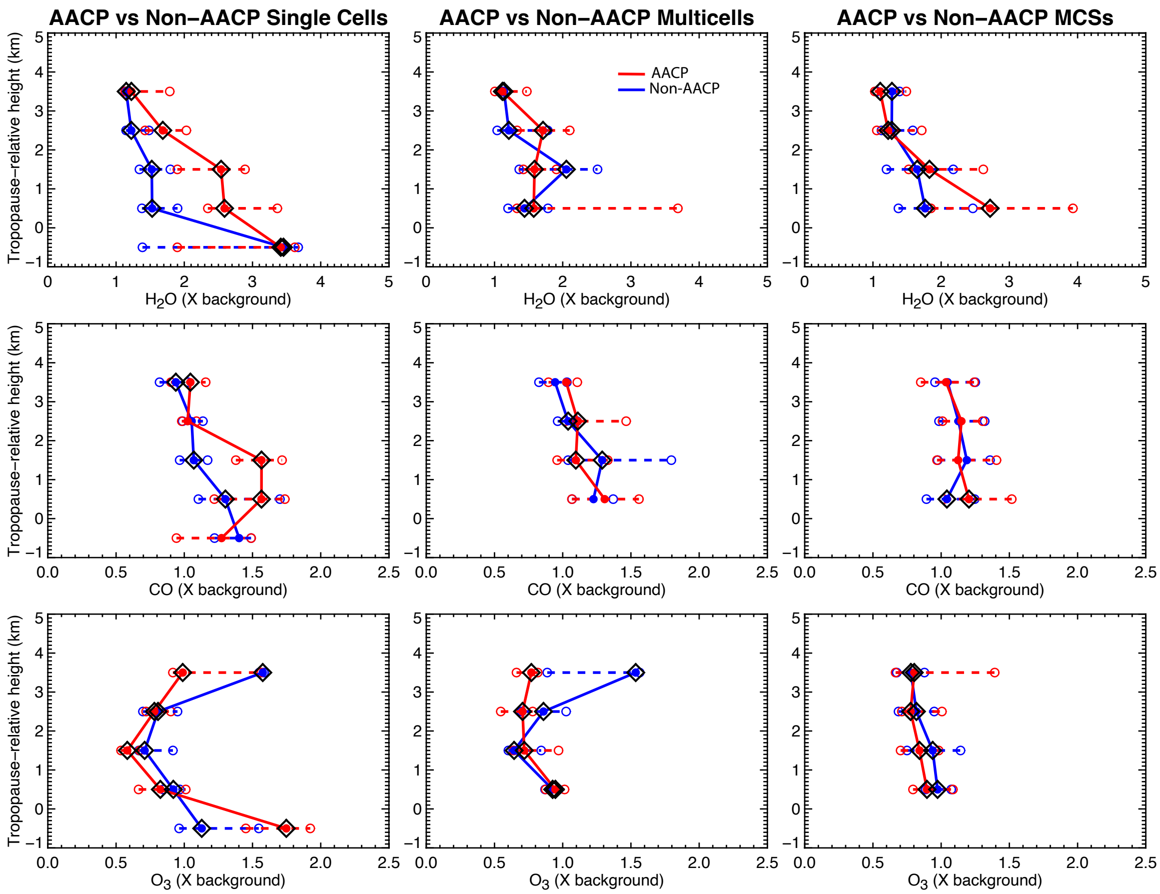

Figure 3.2: As in Fig. 3.1, but for AACP vs. non-AACP (left-to-right) single cell, multicell, and MCS storms.

Zrel (km)	**AACP**	**Non-AACP**	**Single AACP (non-AACP)**	**Multi AACP (non-AACP)**	**MCS AACP (non-AACP)**	**All storms**
4–5	157	167	0(6)	5(3)	152(158)	324
3–4	1604	1026	734(374)	387(296)	483(356)	2630
2–3	3412	3825	498(919)	624(1144)	2290(1762)	7237
1–2	4250	3648	1651(1439)	1164(1043)	1435(1166)	7898
0–1	3727	2987	1547(1248)	407(1101)	1773(638)	6714
-1–0	454	532	347(478)	107(54)	0(0)	986

Table 3.1: Number of 1-second H_2O samples within convective features for each tropopause relative altitude bin used in figures 3.1 – 3.4. O_3 sample sizes are very similar and CO sample sizes are about 10% as large as those listed.

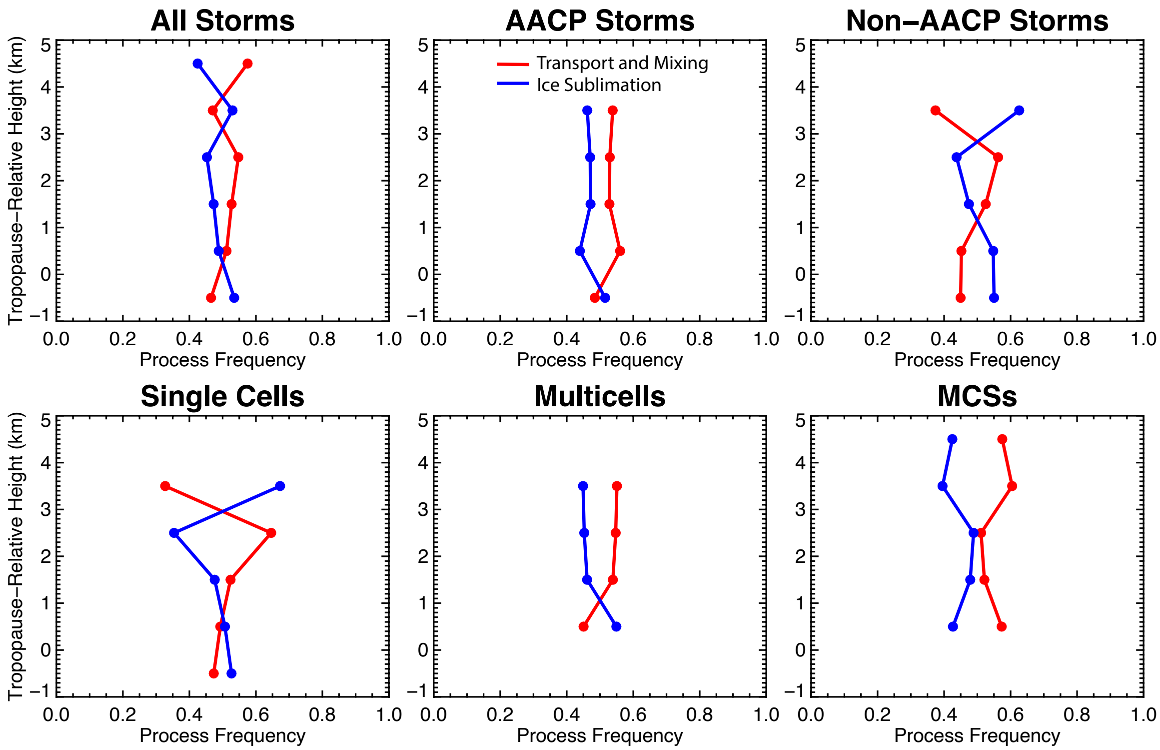

Figure 3.3: Diagnosed air transport & mixing vs. ice sublimation H_2O delivery frequencies as a function of tropopause-relative height for (top left) all storms, (top center) AACP storms, (top right) non-AACP storms, (bottom left) single cells, (bottom center) multicells, and (bottom right) MCSs. Frequencies are calculated based on samples within each 1-km relative altitude bin. For each bin, results are shown only if $\geq$180 s of convective feature sampling occurred.

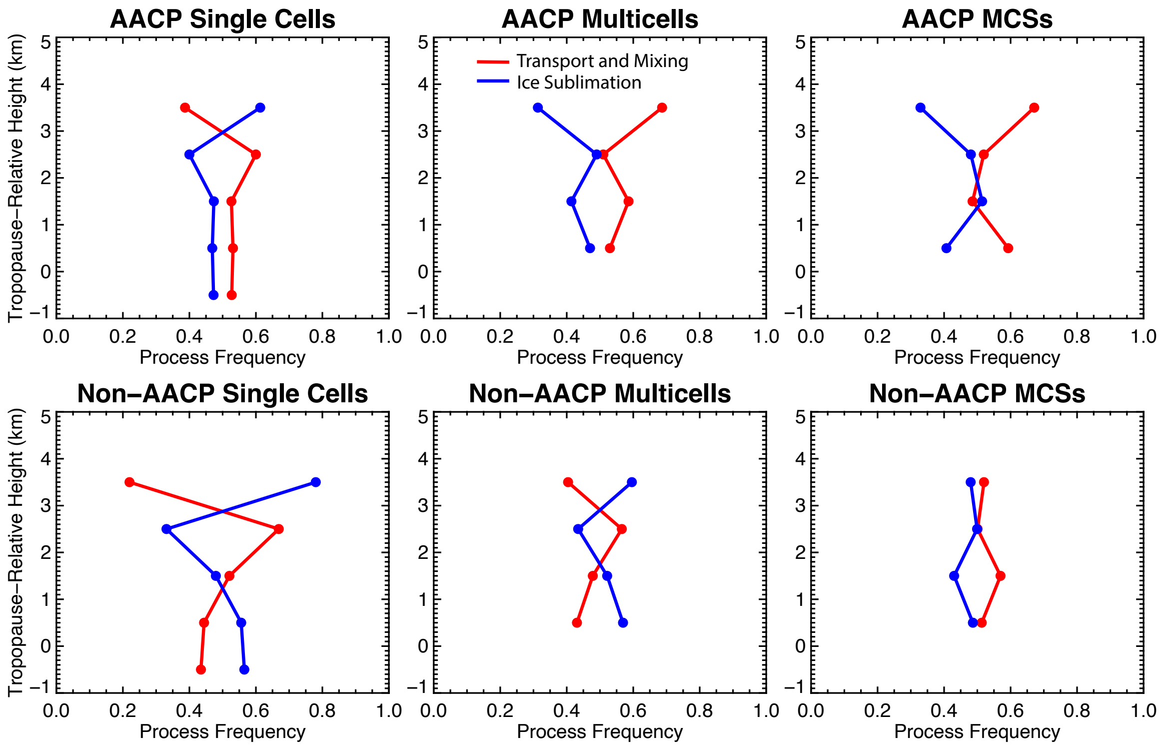

Figure 3.4: As in Fig. 3.3, but for (top) AACP storms and (bottom) non-AACP storms partitioned by storm mode for (left) single cells, (middle) multicells, and (right) MCSs.

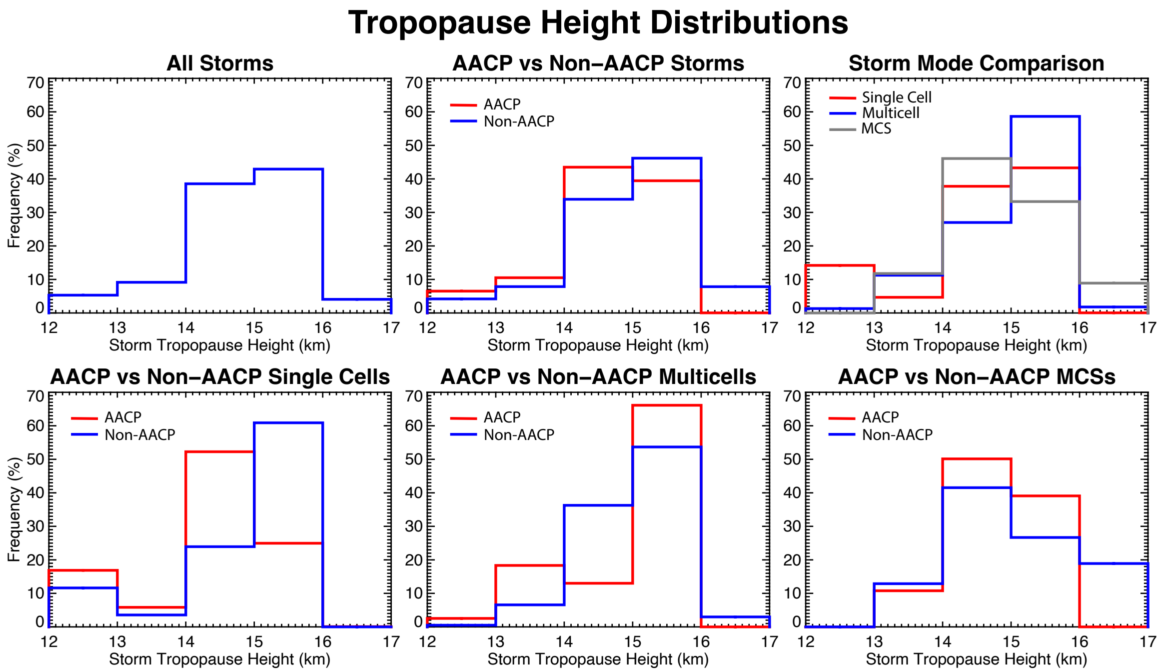

Figure 3.5: Distributions of storm minimum tropopause heights plotted as frequencies for all storms (top left), AACP vs non-AACP storms (top center), different storm modes (top right), and AACP vs non-AACP storms within each separate storm mode (bottom). Differences among distributions were statistically significant in all cases.

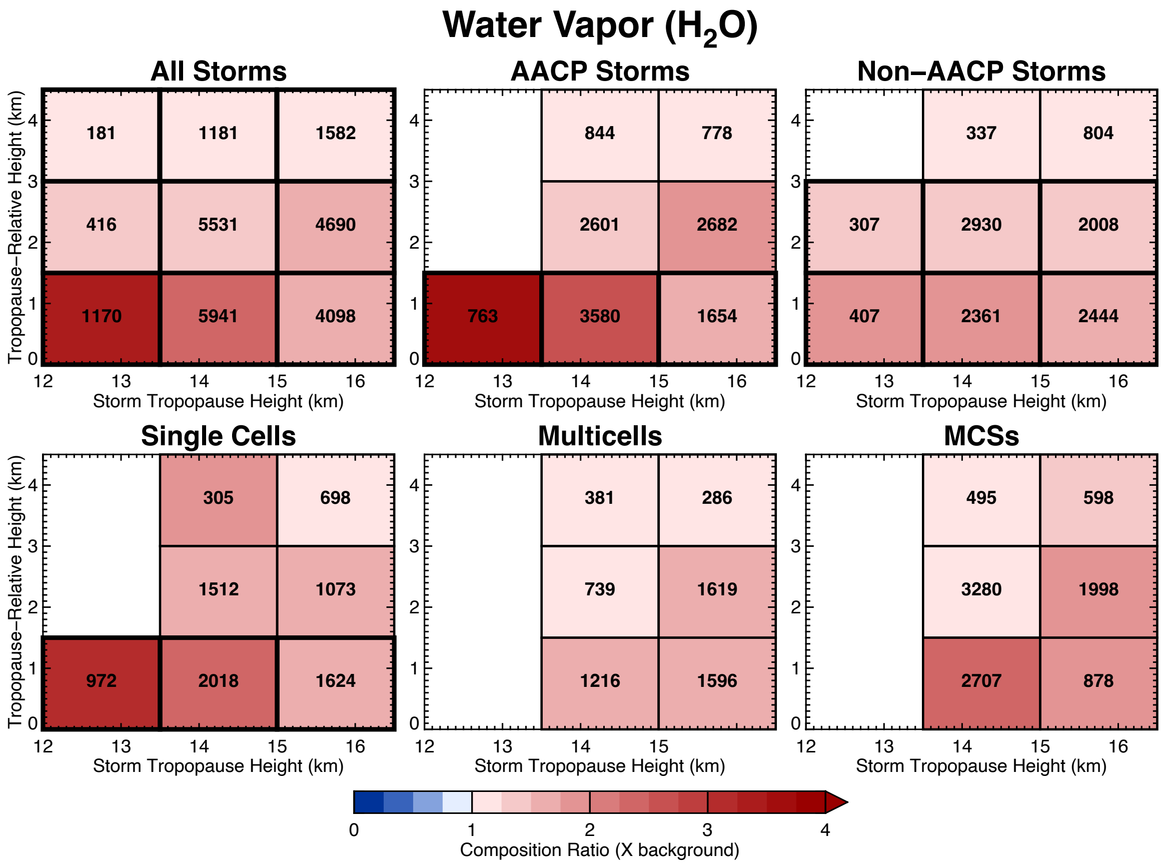

Figure 3.6: Two-dimensional analysis of H_2O enhancement as a function of tropopause-relative height of the flight observation on the vertical axis and storm tropopause height on the horizontal axis for (top left) all storms, (top center) AACP storms, (top middle) non-AACP storms, (bottom left) single cells, (bottom middle) multicells, and (bottom right) MCSs. The color fill represents median background-relative H_2O concentrations. For each bin, results are shown only when $\geq$180 s of convective feature sampling occurred. Numbers within each bin denote the actual number of H_2O measurements that occurred. Thick outlines indicate statistically significant differences between observations in one bin and observations in both other tropopause height bins at the same tropopause relative altitude. Thin outlines indicate significant differences from one of the other bins.

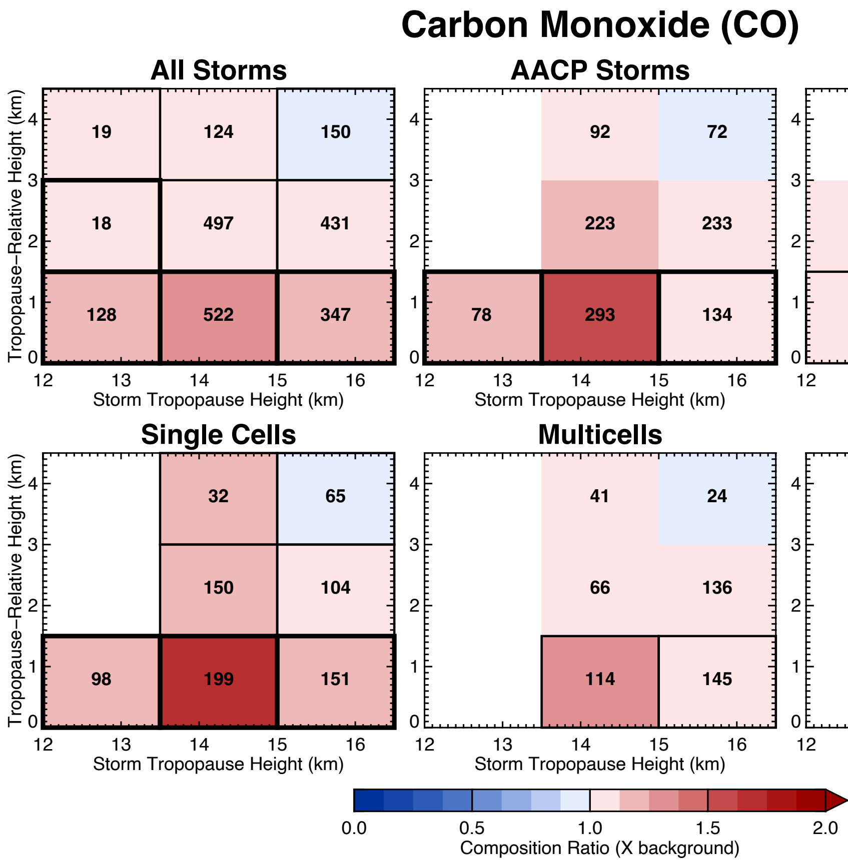

Figure 3.7: As in Fig. 3.6, but for CO.

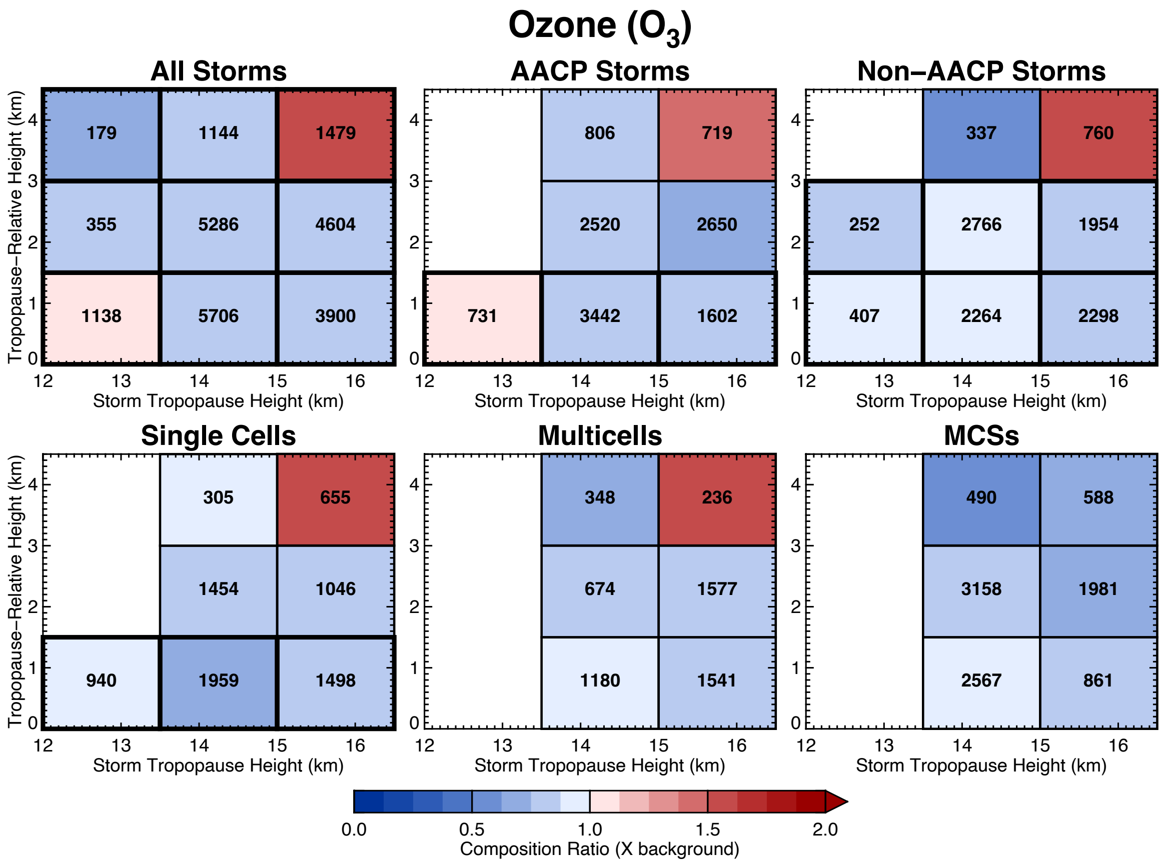

Figure 3.8: As in Fig. 3.9, but for O_3.

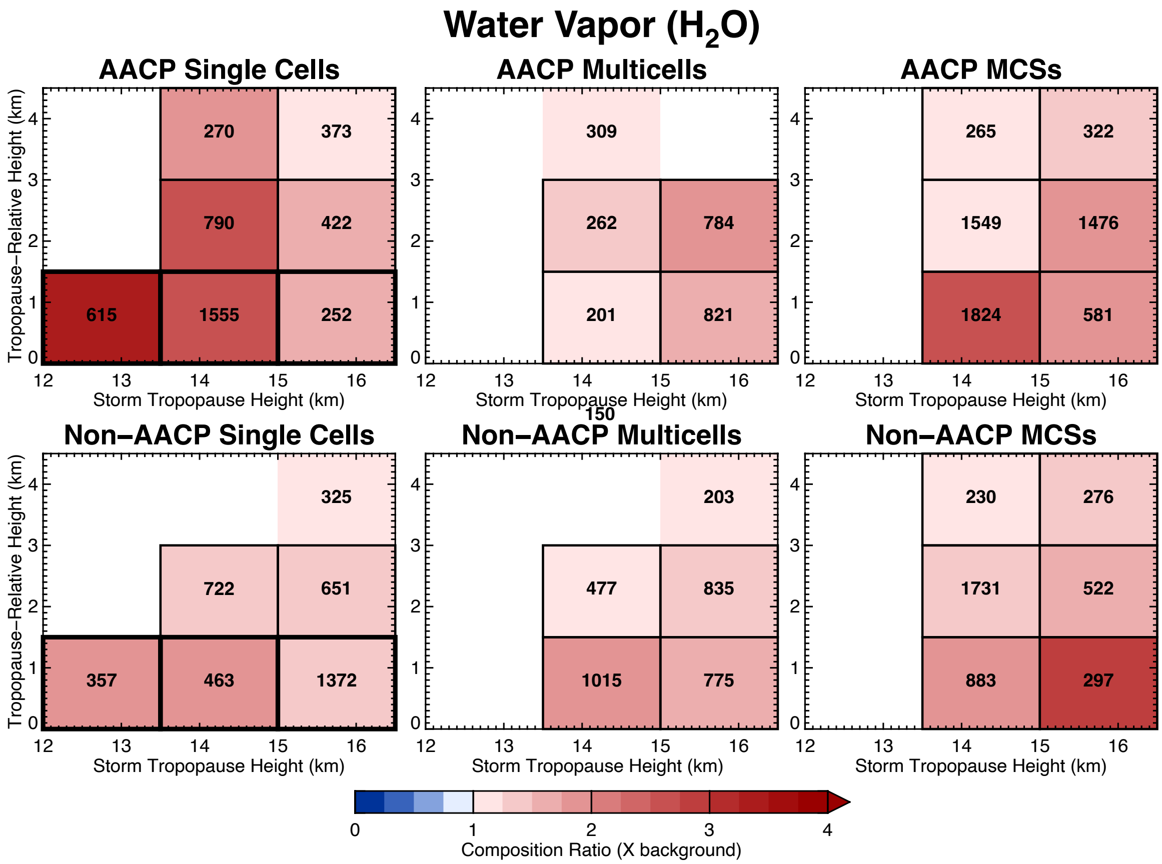

Figure 3.9: As in Fig. 3.6, but for (top) AACP storms and (bottom) non-AACP storms partitioned by storm mode for (left) single cells, (middle) multicells, and (right) MCSs.

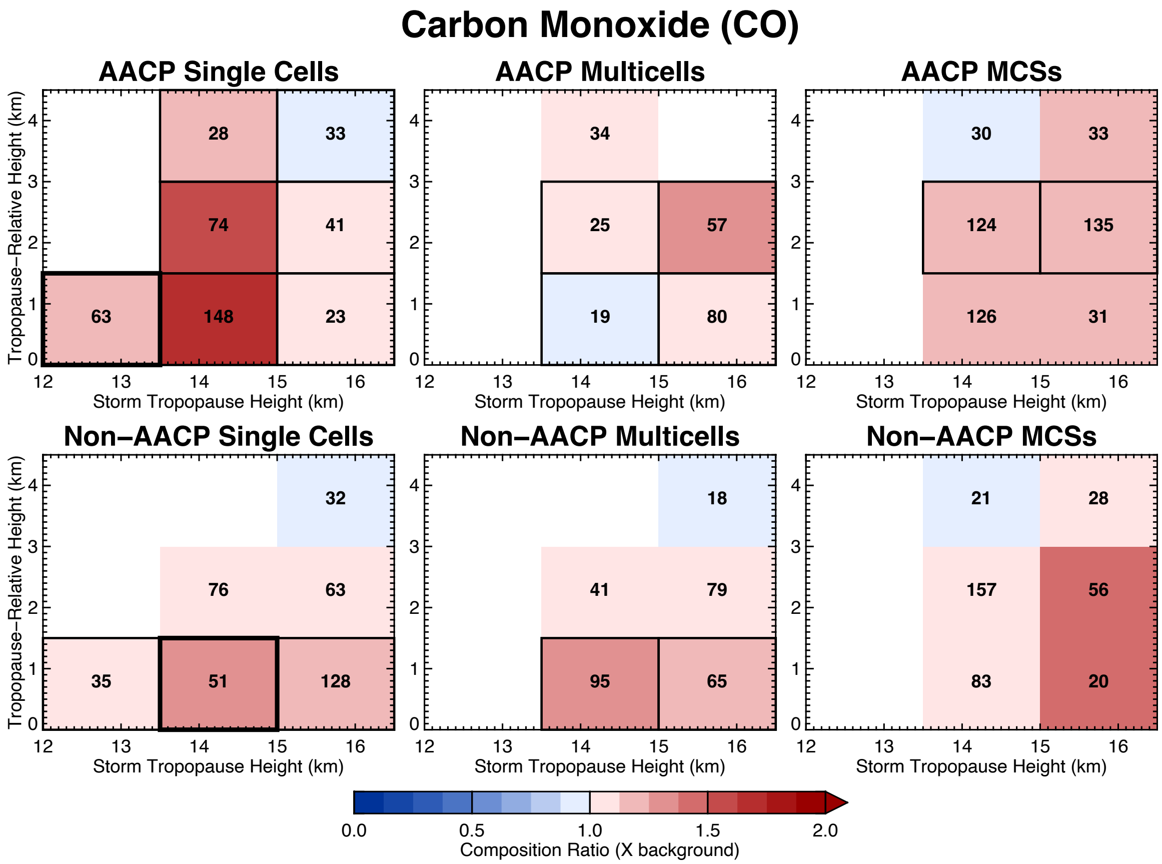

Figure 3.10: As in Fig. 3.6, but for CO.

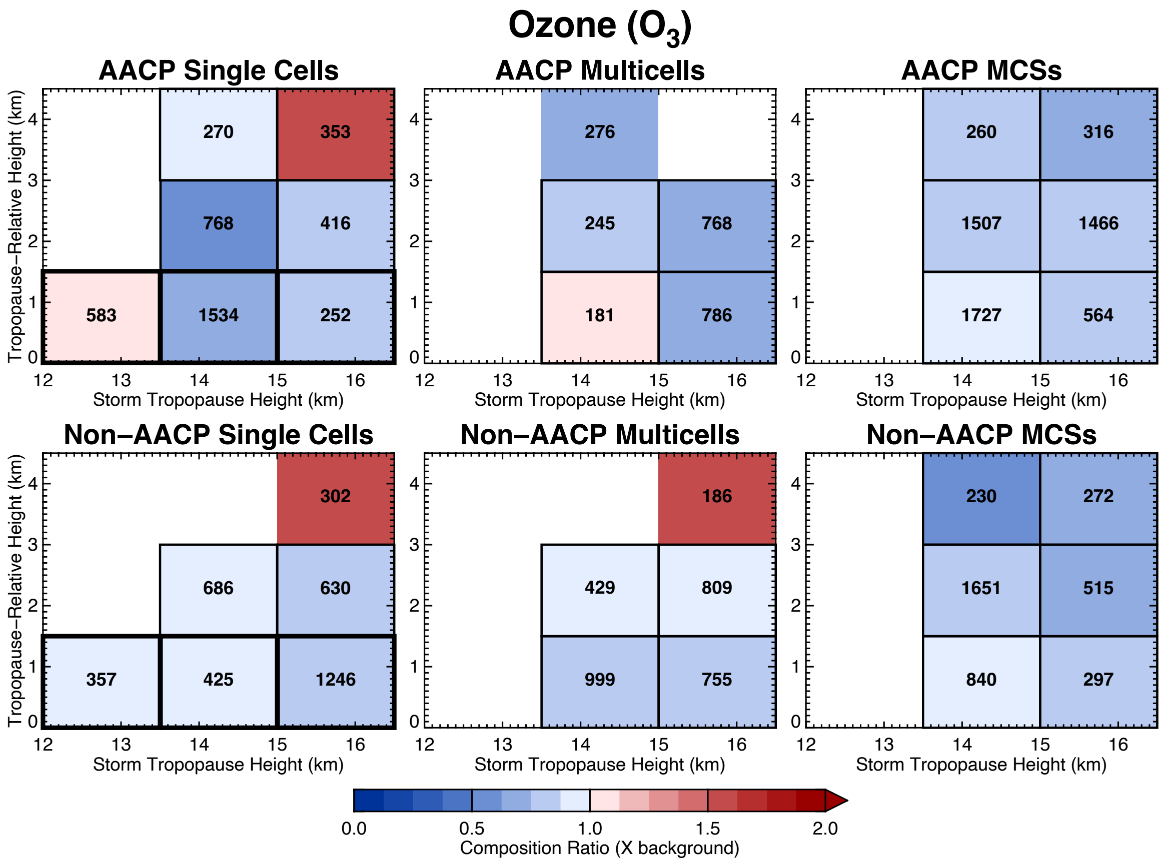

Figure 3.11: As in Fig. 3.9, but for O_3.

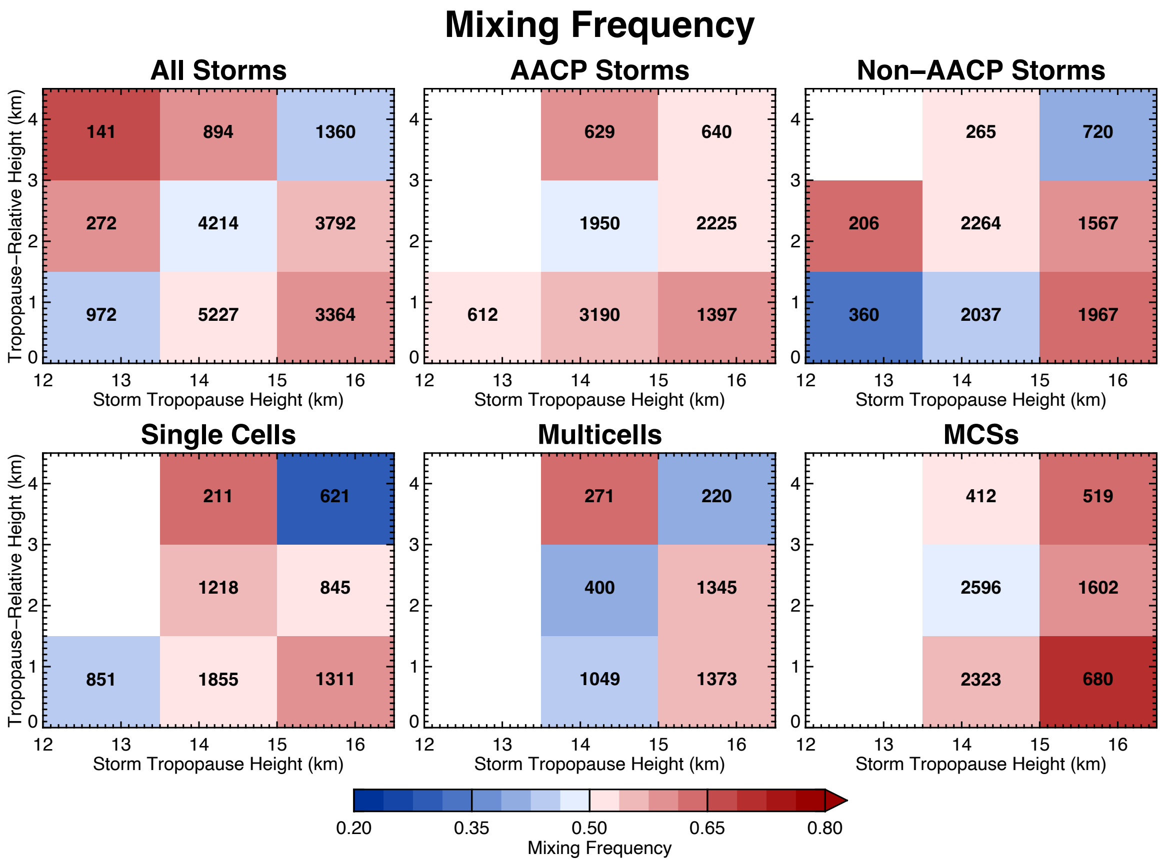

Figure 3.12: Two-dimensional analysis stratospheric hydration process frequencies as a function of tropopause-relative height of the flight observation on the vertical axis and storm tropopause height on the horizontal axis for (top left) all storms, (top center) AACP storms, (top middle) non-AACP storms, (bottom left) single cells, (bottom middle) multi-cells, and (bottom right) MCSs. The color fill represents the frequency of air transport & mixing. For each bin, results are shown only when $\geq$180 s of convective feature sampling occurred. Numbers within each bin denote the actual number of O_3 - H_2O correlations calculated for each bin

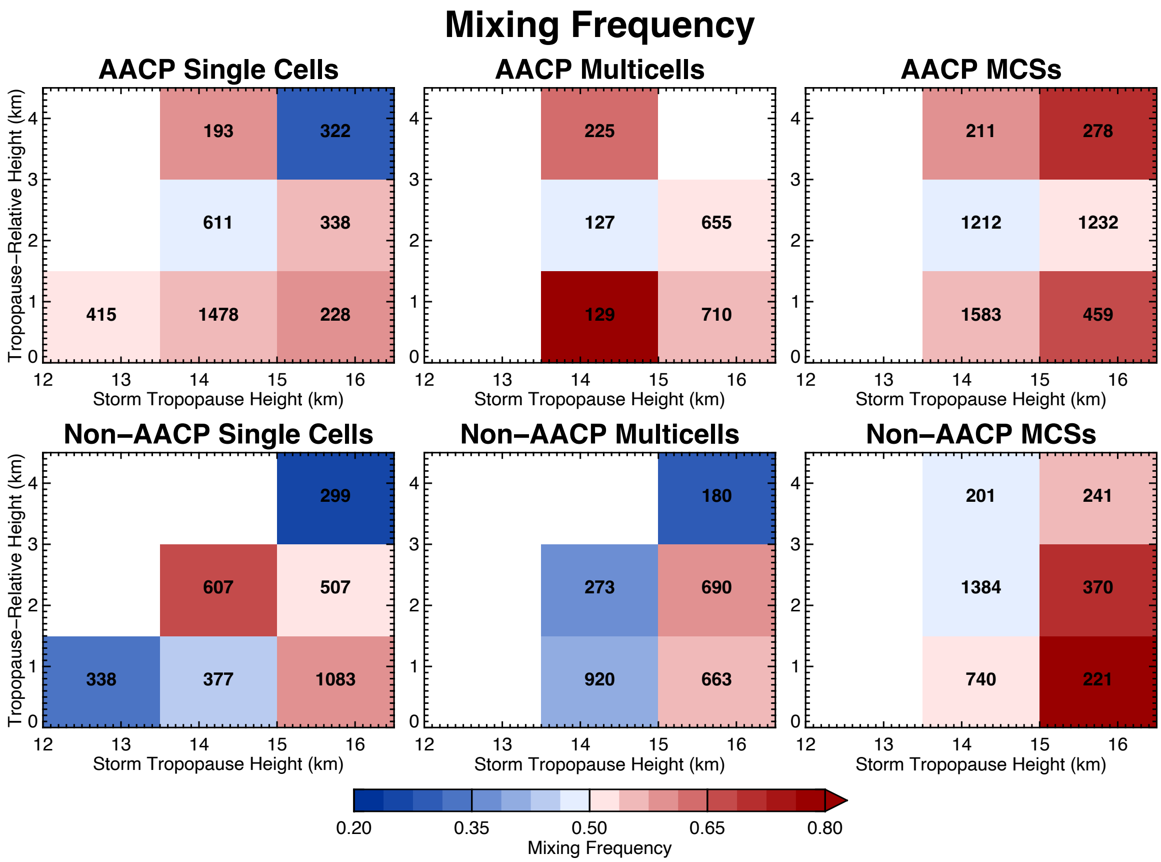

Figure 3.13: As in Fig. 3.12, but for (top) AACP storms and (bottom) non-AACP storms partitioned by storm mode for (left) single cells, (middle) multicells, and (right) MCSs.

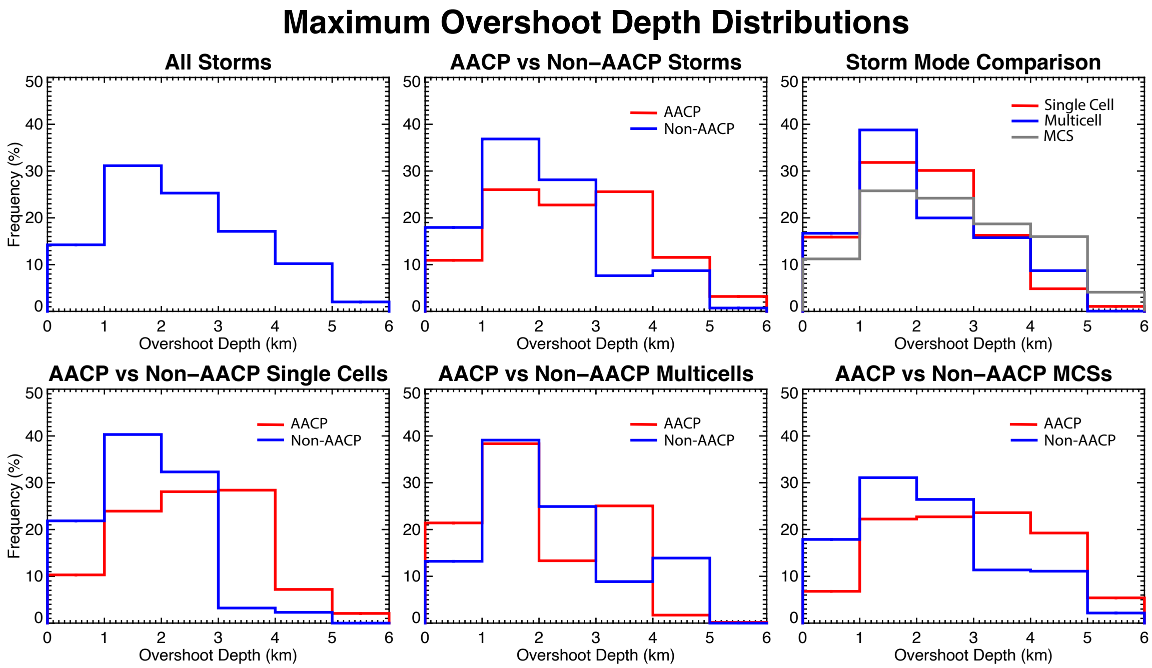

Figure 3.14: Frequency distributions of storm-maximum overshoot depth for (top left) all storms, (top center) AACP vs. non-AACP storms, (top right) different storm modes, and (bottom) AACP vs non-AACP storms within each separate storm mode. Differences among distributions were statistically significant in all cases.

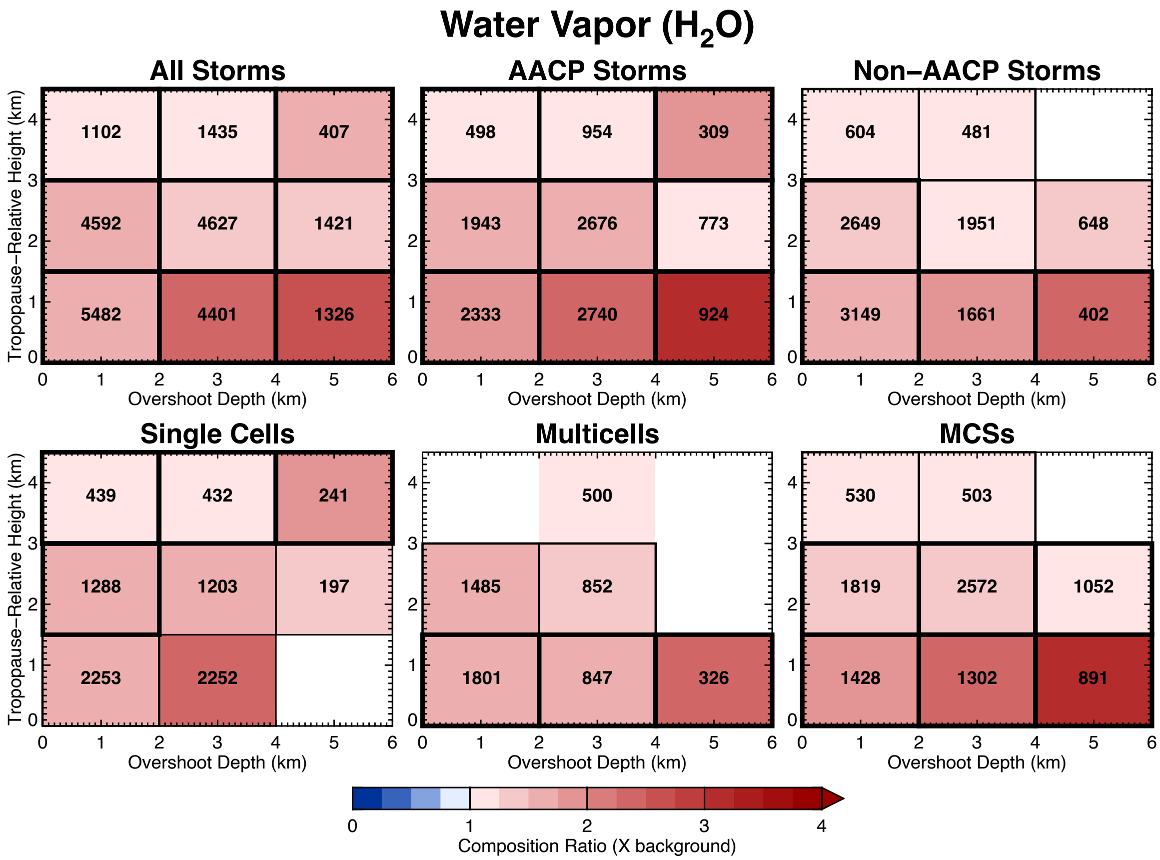

Figure 3.15: As in Fig. 3.6, but as a function of tropopause-relative height of the flight observation on the vertical axis and storm-maximum overshoot depth on the horizontal axis.

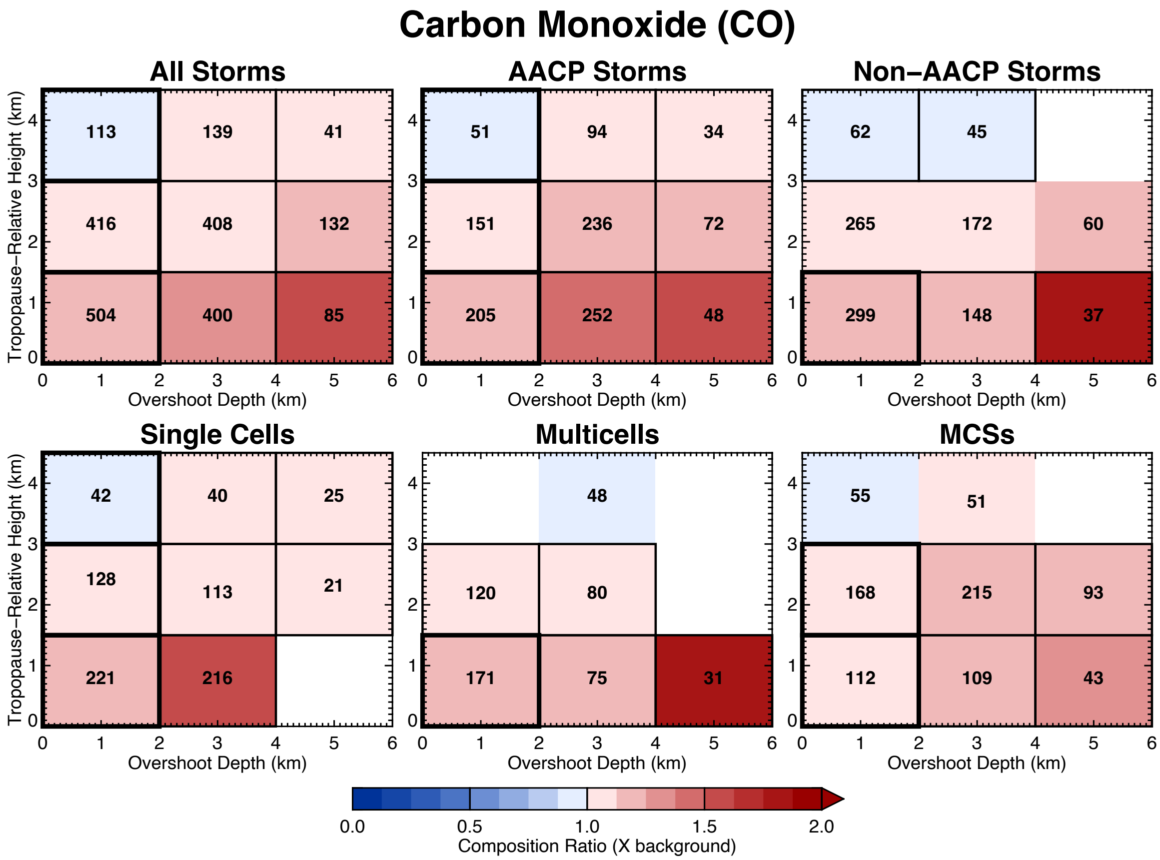

Figure 3.16: As in Fig. 3.15, but for CO.

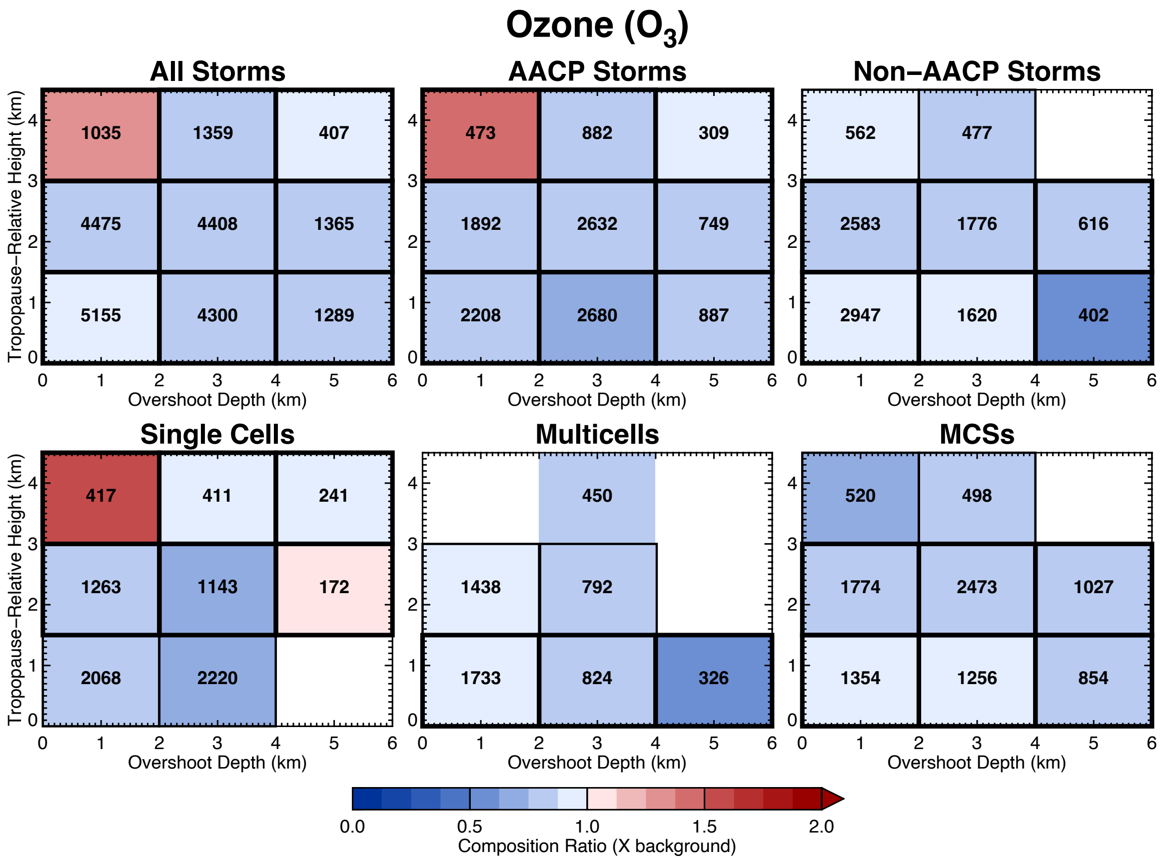

Figure 3.17: As in Fig. 3.15, but for O_3.

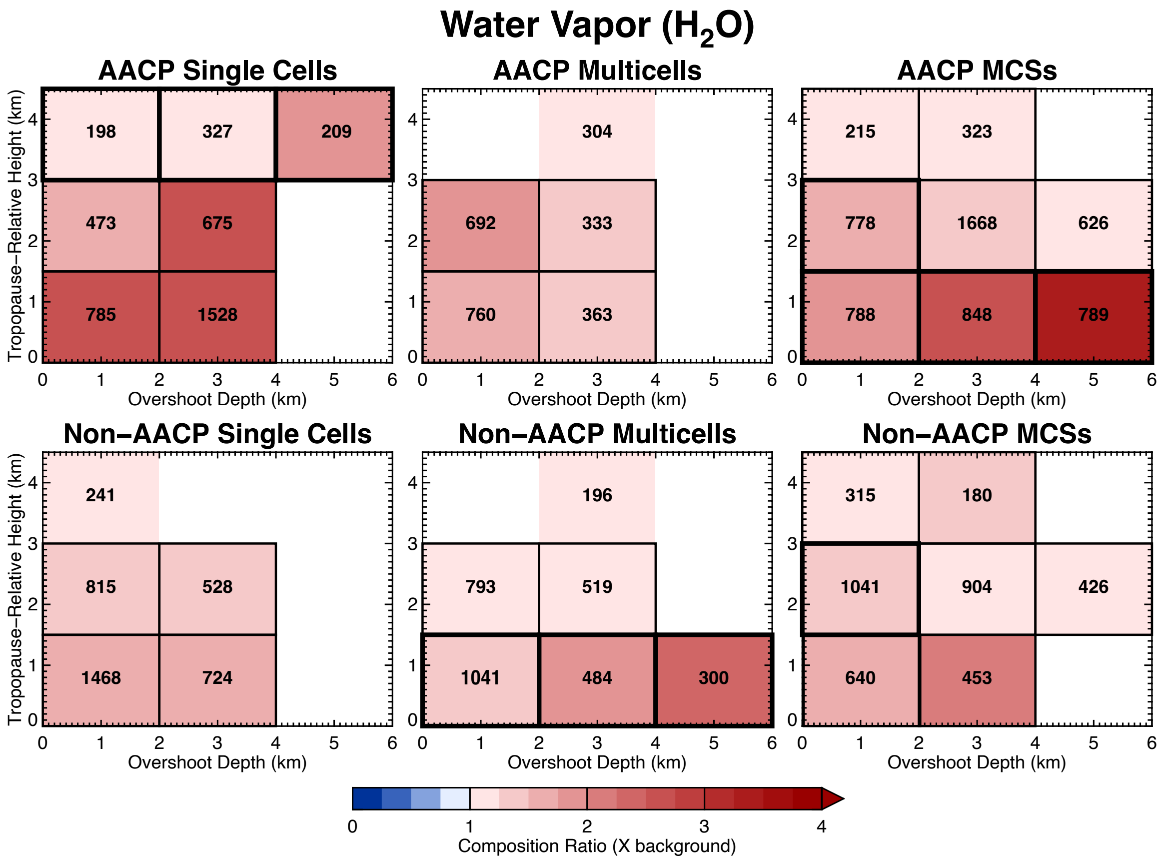

Figure 3.18: As in Fig. 3.15, except that median background relative H_2O concentrations in each bin are displayed for AACP single cells (top left), AACP multicells (top center), AACP MCSs (top right), non-AACP single cells (bottom left), non-AACP multicells (bottom center), and non-AACP MCSs (bottom right) separately.

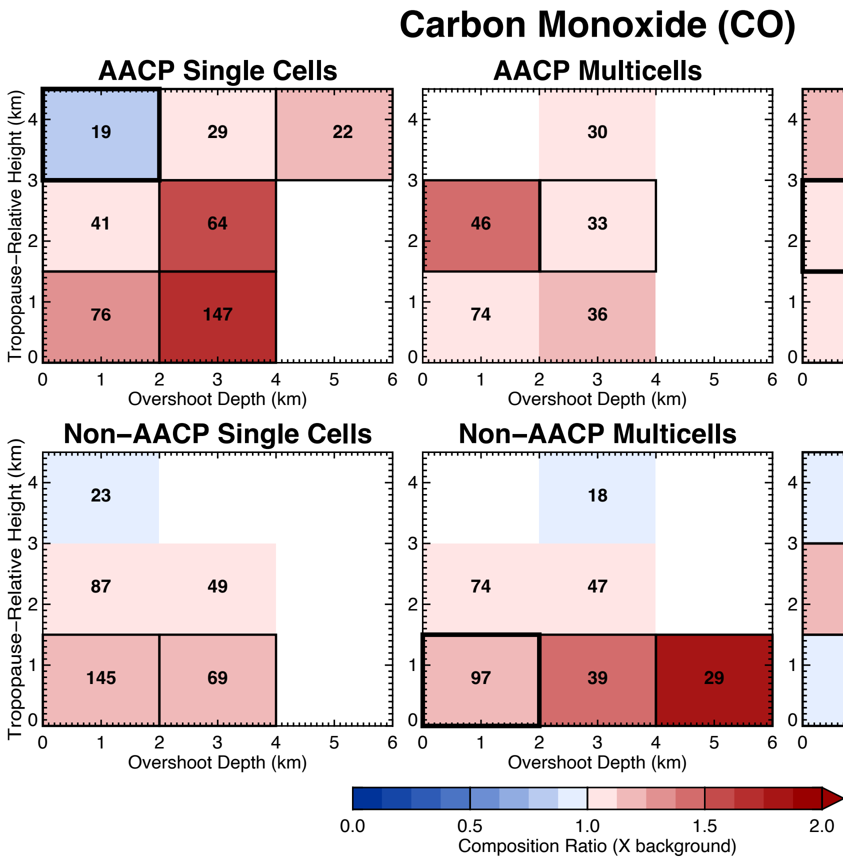

Figure 3.19: As in Fig. 3.18 but for CO

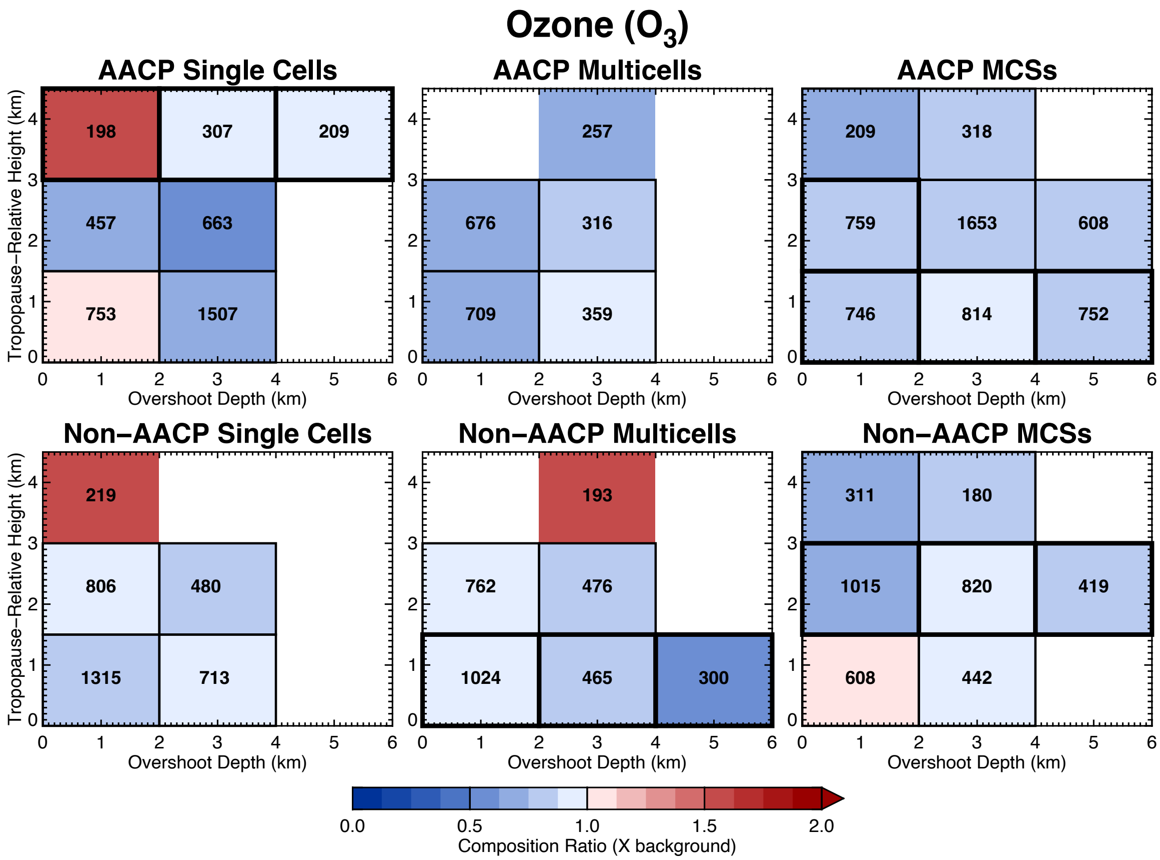

Figure 3.20: As in Fig. 3.18 but for O_3

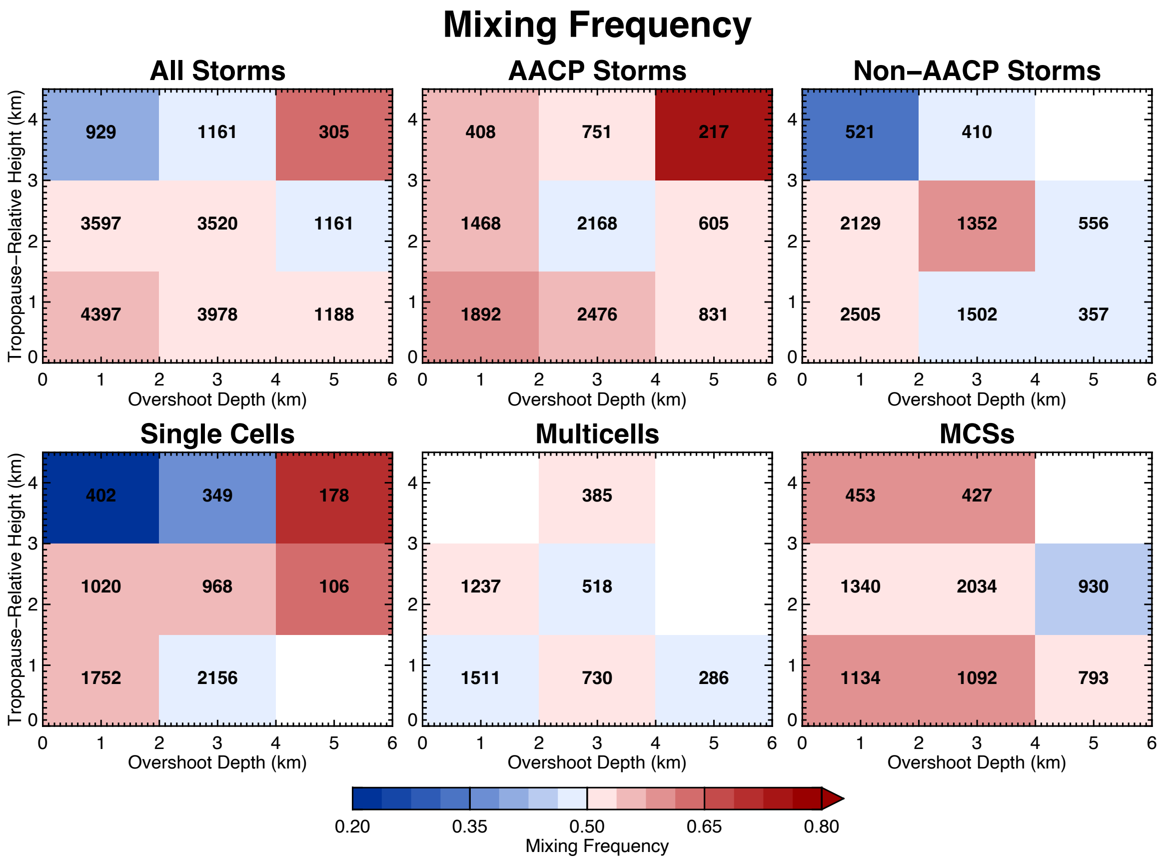

Figure 3.21: As in Fig. 3.12, but with overshoot depth on the horizontal axis.

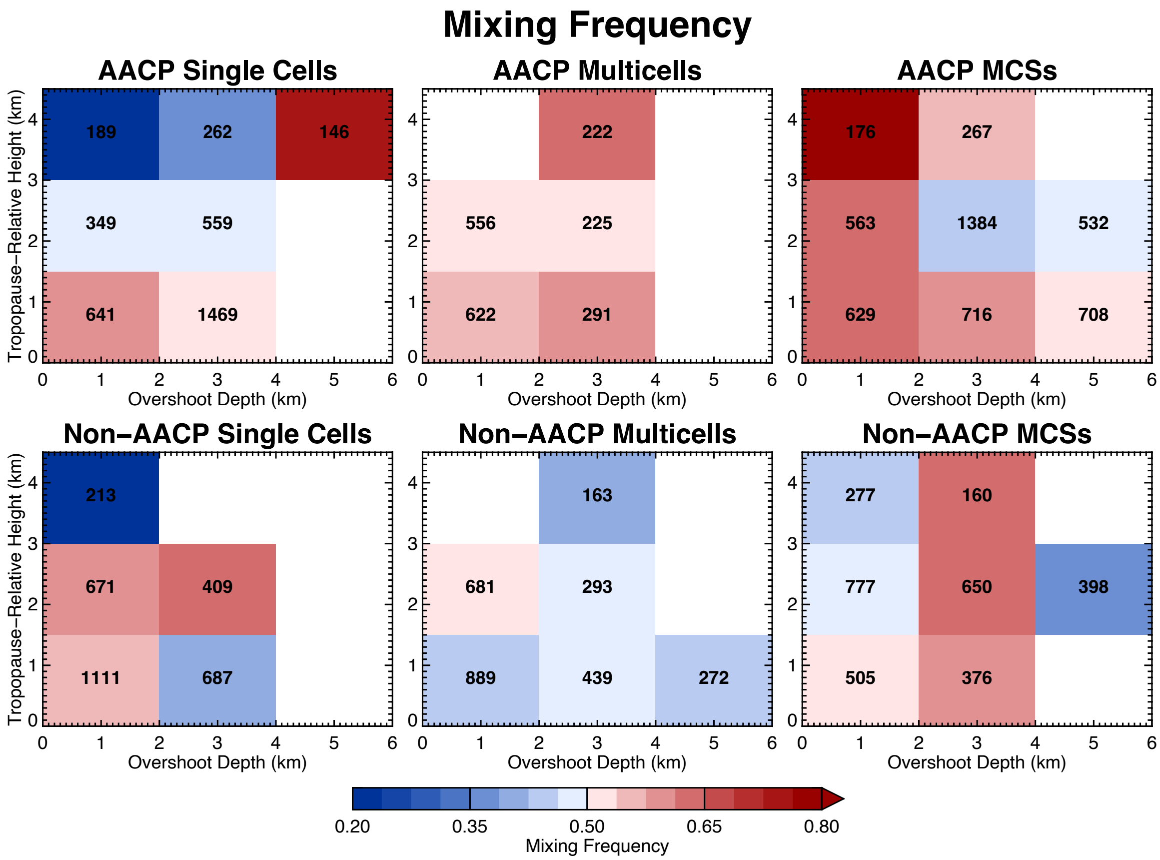

Figure 3.22: As in Fig. 3.21, but for (top) AACP storms and (bottom) non-AACP storms partitioned by storm mode for (left) single cells, (middle) multicells, and (right) MCSs.

Chapter 4

Summary and discussion

This study utilizes an extensive dataset of in-situ observations from the DCOTSS field campaign to evaluate relationships between storm & environmental characteristics and TST within overshooting storms. It is the first such effort involving a large-scale observational dataset. Trajectory calculations are employed in conjunction with radar, satellite and reanalysis data to link aircraft observations of stratospheric composition change to individual overshooting storms and evaluate the attributes of those storm and their environments. We sort each matched storm into one of six categories for comparison: AACP single cells, non-AACP single cells, AACP multicells, non-AACP multicells, AACP MCSs, and non-AACP MCSs. We also investigate stratospheric hydration processes (air transport and mixing versus ice sublimation) using O3-H_2O and θ-H_2O correlations. Our results provide further evidence that convection over the continental U.S. drives frequent and substantial stratospheric hydration through both injection of tropospheric air and sublimation of ice crystals. We observe this hydration from different types of storms in a variety of environments. We also document substantial transport of the mostly passive gases CO and O_3. Although not a focus of our study, STT is also conditionally observed via O_3 enhancements in the upper troposphere. Our results also clearly demonstrate the different transport characteristics of H_2O and CO which have been documented in numerous prior studies. First, H_2O is transported to greater altitudes than CO throughout the DCOTSS dataset. Second, the impact of saturation limits on H_2O transport (versus no saturation limits on CO transport) is apparent throughout. These limits especially impact the hydration potential of AACP storms, in agreement with Gordon et al. (2024). Third, our analysis clearly demonstrates that storms with AACPs produce much greater TST compared to those without AACPs. While this result is unsurprising, it verifies prior modeling and observational results on a larger scale.

While prior modeling studies agreed that AACPs produced stronger hydration at deeper levels in the stratosphere, disagreement existed as to whether AACPs led to greater hydration in the LMS (Homeyer et al. 2017; O'Neill et al. 2021; Gordon and Homeyer 2022). The DCOTSS observations indicate that AACP effects for all trace gases are actually maximized just above the tropopause (especially for non-discrete storms). Furthermore, these prior modeling studies all simulated discrete supercells, whereas our analysis includes non-supercellular convection and involves both discrete storms and convective complexes. Our results demonstrate that AACPs produce the largest impacts in single-cell storms. Meanwhile, AACP effects are limited to the first 1-2 km above the tropopause for other modes, which could result from AACPs having shorter lifetimes in such cases (Bedka et al. 2018). Tracer-tracer analysis illustrates a predominance of mixing in AACP storms, while mixing frequency dominates in a narrower range (1-3 km above the tropopause) in non-AACP storms. AACP storms also produce greater O_3 enhancements in the upper troposphere.

Storm mode also impacts the magnitude and depth of TST. While much of the difference among modes can be attributed to AACPs, some subtle differences still appear when removing AACP effects. For example, MCSs exhibit increased hydration near the tropopause and increased CO transport at higher tropopause-relative altitudes. Tracer-tracer analysis also reveals greater mixing frequency for MCSs compared to other modes at both low and high altitudes, which helps explain the deeper CO transport.

We also explore the impact of other environmental variables on TST. Relationships between TST and tropopause height & storm maximum overshoot depth yield meaningful and interesting results. We utilize two-dimensional analysis to examine both the magnitude and depth of composition changes at various tropopause heights and overshoot depths. This reveals that H_2O and CO enhancements are greatest in low to medium tropopause environments in the first 1.5 km above the tropopause. As tropopause heights increase, hydration near the tropopause decreases, but hydration at higher relative altitudes is less impacted. In contrast, CO transport decreases with altitude and becomes negligible at higher tropopause-relative altitudes in high tropopause environments. Examining mixing versus sublimation frequencies provides an explanation for this difference, revealing that the stratospheric depth of air transport and mixing decreases as tropopause height increases, while ice sublimation can still occur at higher altitudes. Our analysis also illustrates a greater impact of tropopause height on TST among AACP storms, especially AACP single cells, demonstrating the importance of tropopause height in modulating the impact of AACPs on TST. Meanwhile, single cells produce greater TST in lower tropopause environments, and MCSs produce greater TST in higher tropopause environments, with multicells sharing characteristics of both other modes.

Examining patterns of H_2O and CO transport against storm overshoot depth demonstrates that greater overshoot depth increases both the magnitude and depth of TST (via air transport and mixing), though evidence of saturation constraints on hydration becomes apparent at higher overshoot depth. Among MCSs, sublimation frequency is elevated over air transport and mixing at the highest overshoot depths, despite CO observations displaying an increase in absolute transport and mixing, indicating that a very large amount of sublimation must have occurred with these MCSs. These results somewhat resolve the disagreement among prior modeling studies over whether overshoot depth significantly affects the magnitude of hydration (Dauhut et al. 2018; Phoenix and Homeyer 2021), though the hypothesis proposed for increased hydration at higher overshoot depths proposed in (Dauhut et al. 2018) may not be the dominant mechanism outside of MCSs.

O_3 perturbations reveal that entrainment of stratospheric air into the overshoot frequently occurs in higher tropopause environments, particularly for discrete storms with shallow overshooting. This entrainment is accompanied by high sublimation frequencies, indicating that the infusion of warmer and drier air engenders rapid ice sublimation. MCSs are the only mode that do not exhibit this entrainment in high tropopause environments, which may explain why concentrations of H_2O and CO are greater in higher tropopause environments for MCSs. Perhaps greater storm coverage and accompanying upward transport of tropospheric air shields updrafts from this entrainment or the dynamical mechanisms responsible are less likely to be induced.

Taken together, our results comparing different storm modes suggest that MCSs can promote larger stratospheric composition change in high tropopause environments. In these environments, where the strongest overshoots reach less deeply into the stratosphere and transport is more saturation-limited, the more voluminous transport facilitated by MCSs appears to outweigh the stronger transport within discrete updrafts. Conversely, discrete cells produce greater transport only in lower to medium tropopause environments, mainly when an AACP is present. These higher tropopause environments are located equatorward of the subtropical jet, meaning the injected air may be more likely to circulate within the NAMA; therefore, MCSs may have greater cumulative long-term impacts on stratospheric composition over North America despite the capability of single-cell storms (especially AACP-producing) to introduce extreme stratospheric perturbations in lower tropopause environments. These results add nuance to the modeling results of Bigelbach et al. (2014), which showcased stronger transport per unit area in single cells compared to MCSs but did not discriminate between AACP vs non-AACP storms or different tropopause environments. Perhaps their results are mainly driven by AACP storms and/or storms in lower tropopause environments. Other sample biases may also complicate the picture. For instance, our single cell population in high tropopause environments may simply involve weaker cases than that of Bigelbach et al. (2014), on average. There were relatively few supercells sampled during DCOTSS, and previous model simulations have suggested that supercells have the strongest transport and the highest detrainment levels of any storm type (Mullendore et al. 2005, 2013), so a lack of supercells could easily skew the single cell population toward weaker transport values. Furthermore, Bigelbach et al. (2014) explicitly excluded weaker cases from their analysis. Perhaps supercells have the strongest and deepest transport, followed by MCSs, while non-supercellular discrete convection exhibits the weakest transport. Future efforts could shed further light on our results by comparing stratospheric composition changes resulting from supercellular versus non-supercellular single cells and MCSs.

This study raises a number of hypotheses to explain the results apparent in the observational data; however, our ability to test the validity of these explanations is limited. Furthermore, our comparisons among different storm types are subject to sample biases. Future work conducting model simulations of H_2O and tracer transport within various matched storms from our dataset could help shed further light on transport characteristics occurring under different storm and environmental conditions and delineate which results are most robust. We also focus only on the magnitude and depth of trace gas perturbations, rather than the spatial extent of these perturbations. As such, we cannot estimate which conditions lead to greater total mass transport or STE. For instance, AACP single cells may produce extreme enhancements in localized areas, whereas MCSs produce weaker enhancements but likely on a much larger scale due to size of the convective system. Model simulations could be combined with our observations to estimate total CO and H_2O fluxes from different storm types under varying environmental conditions. These calculations could then be combined with radar- and satellite-based climatologies of overshooting storms in different tropopause environments to determine which types of storms contribute most to stratospheric composition change over North America. Despite its limitations, this study provides an unprecedented analysis of in situ observations, showcasing ways in which different storm and environmental characteristics can impact the magnitude and depth of stratospheric composition changes associated with convection.

Bibliography

Adler, R. F., and R. A. Mack, 1986: Thunderstorm cloud top dynamics as inferred from satellite observations and a cloud top parcel model. *Journal of Atmospheric Sciences*, **43 (18)**, 1945 – 1960, https://doi.org/10.1175/1520-0469(1986)043⟨1945:TCTDAI⟩2.0.CO;2, URL https://journals.ametsoc.org/view/journals/atsc/43/18/1520-0469_1986_043_1945_tctdai_2_0_co_2.xml.

Anderson, J. G., D. M. Wilmouth, J. B. Smith, and D. S. Sayres, 2012: Uv dosage levels in summer: Increased risk of ozone loss from convectively injected water vapor. *Science*, **337 (6096)**, 835–839, https://doi.org/10.1126/science.1222978, URL https://www.science.org/doi/abs/10.1126/science.1222978, https://www.science.org/doi/pdf/10.1126/science.1222978.

Anderson, J. G., and Coauthors, 2017: Stratospheric ozone over the united states in summer linked to observations of convection and temperature via chlorine and bromine catalysis. *Proceedings of the National Academy of Sciences*, **114 (25)**, E4905–E4913, https://doi.org/10.1073/pnas.1619318114, URL https://www.pnas.org/doi/abs/10.1073/pnas.1619318114, https://www.pnas.org/doi/pdf/10.1073/pnas.1619318114.

Auth, R. M., and C. R. Homeyer, 2023: Targeted balloon observations of stratosphere-to-troposphere transport from a mesoscale convective system. *Journal of Geophysical Research: Atmospheres*, **128 (16)**, e2023JD039 139, https://doi.org/https://doi.org/10.1029/2023JD039139, URL https://agupubs.onlinelibrary.wiley.com/doi/abs/10.1029/2023JD039139, e2023JD039139 2023JD039139, https://agupubs.onlinelibrary.wiley.com/doi/pdf/10.1029/2023JD039139.

Ban-Weiss, G., L. Cao, M. Previdi, G. Bala, and K. Caldeira, 2012: Dependence of climate forcing and response on the altitude of black carbon aerosols. *Climate Dynamics*, **38**, 897–911, https://doi.org/10.1007/s00382-019-04721-4.

Banerjee, A., G. Chiodo, M. Previdi, M. Ponater, A. J. Conley, and L. M. Polvani, 2019: Stratospheric water vapor: an important climate feedback. *Climate Dynamics*, **53**, 1697–1710, https://doi.org/10.1007/s00382-019-04721-4.

Barth, M. C., and Coauthors, 2015: The deep convective clouds and chemistry (dc3) field campaign. *Bulletin of the American Meteorological Society*, **96 (8)**, 1281 – 1309, https://doi.org/10.1175/BAMS-D-13-00290.1, URL https://journals.ametsoc.org/view/journals/bams/96/8/bams-d-13-00290.1.xml.

Bedka, K., E. M. Murillo, C. R. Homeyer, B. Scarino, and H. Mersiovsky, 2018: The above-anvil cirrus plume: An important severe weather indicator in visible and infrared satellite imagery. *Weather and Forecasting*, **33 (5)**, 1159 – 1181, https://doi.org/10.1175/WAF-D-18-0040.1, URL https://journals.ametsoc.org/view/journals/wefo/33/5/waf-d-18-0040_1.xml.

Bedka, K. M., C. Wang, R. Rogers, L. D. Carey, W. Feltz, and J. Kanak, 2015: Examining deep convective cloud evolution using total lightning, wsr-88d, and goes-14 super rapid scan datasets*. *Weather and Forecasting*, **30 (3)**, 571 – 590, https://doi.org/10.1175/WAF-D-14-00062.1, URL https://journals.ametsoc.org/view/journals/wefo/30/3/waf-d-14-00062_1.xml.

Bigelbach, B. C., G. L. Mullendore, and M. Starzec, 2014: Differences in deep convective transport characteristics between quasi-isolated strong convection and mesoscale convective systems using seasonal wrf simulations. *Journal of Geophysical Research: Atmospheres*, **119 (19)**, 11,445–11,455, https://doi.org/https://doi.org/10.1002/2014JD021875, URL https://agupubs.onlinelibrary.wiley.com/doi/abs/10.1002/2014JD021875, https://agupubs.onlinelibrary.wiley.com/doi/pdf/10.1002/2014JD021875.

Brewer, A. W., 1949: Evidence for a world circulation provided by the measurements of helium and water vapour distribution in the stratosphere. *Quarterly Journal of the Royal Meteorological Society*, **75 (326)**, 351–363, https://doi.org/https://doi.org/10.1002/qj.49707532603, URL https://rmets.onlinelibrary.wiley.com/doi/abs/10.1002/qj.49707532603, https://rmets.onlinelibrary.wiley.com/doi/pdf/10.1002/qj.49707532603.

Butchart, N., 2014: The brewer-dobson circulation. *Reviews of Geophysics*, **52 (2)**, 157–184, https://doi.org/https://doi.org/10.1002/2013RG000448, URL https://agupubs.onlinelibrary.wiley.com/doi/abs/10.1002/2013RG000448, https://agupubs.onlinelibrary.wiley.com/doi/pdf/10.1002/2013RG000448.

Chaboureau, J.-P., J.-P. Cammas, J. Duron, P. J. Mascart, N. M. Sitnikov, and H.-J. Voessing, 2007: A numerical study of tropical cross-tropopause transport by convective overshoots. *Atmospheric Chemistry and Physics*, **7 (7)**, 1731–1740, https://doi.org/10.5194/acp-7-1731-2007, URL https://acp.copernicus.org/articles/7/1731/2007/.

Chang, K.-W., K. P. Bowman, and A. D. Rapp, 2023: Transport and confinement of plumes from tropopause-overshooting convection over the contiguous united states during the warm season. *Journal of Geophysical Research: Atmospheres*, **128 (2)**, e2022JD037 020, https://doi.org/https://doi.org/10.1029/2022JD037020, URL https://agupubs.onlinelibrary.wiley.com/doi/abs/10.1029/2022JD037020, e2022JD037020 2022JD037020, https://agupubs.onlinelibrary.wiley.com/doi/pdf/10.1029/2022JD037020.

Charlesworth, E., and Coauthors, 2023: Stratospheric water vapor affecting atmospheric circulation. *Nature Communications*, **14 (3925)**, https://doi.org/https://doi.org/10.1038/s41467-023-39559-2, URL https://www.nature.com/articles/s41467-023-39559-2#author-information.

Chemel, C., M. R. Russo, J. A. Pyle, R. S. Sokhi, and C. Schiller, 2009: Quantifying the imprint of a severe hector thunderstorm during active/scout-o3 onto the water content in the upper troposphere/lower stratosphere. *Monthly Weather Review*, **137 (8)**, 2493 – 2514, https://doi.org/10.1175/2008MWR2666.1, URL https://journals.ametsoc.org/view/journals/mwre/137/8/2008mwr2666.1.xml.

Cooney, J. W., K. P. Bowman, C. R. Homeyer, and T. M. Fenske, 2018: Ten year analysis of tropopause-overshooting convection using gridrad data. *Journal of Geophysical Research: Atmospheres*, **123 (1)**, 329–343, https://doi.org/https://doi.org/10.1002/2017JD027718, URL https://agupubs.onlinelibrary.wiley.com/doi/abs/10.1002/2017JD027718, https://agupubs.onlinelibrary.wiley.com/doi/pdf/10.1002/2017JD027718.

Corti, T., and Coauthors, 2008: Unprecedented evidence for deep convection hydrating the tropical stratosphere. *Geophysical Research Letters*, **35 (10)**, https://doi.org/https://doi.org/10.1029/2008GL033641, URL https://agupubs.onlinelibrary.wiley.com/doi/abs/10.1029/2008GL033641, https://agupubs.onlinelibrary.wiley.com/doi/pdf/10.1029/2008GL033641.

Crosson, E. R., 2008: A cavity ring-down analyzer for measuring atmospheric levels of methane, carbon dioxide, and water vapor. *Applied Physics B*, **92 (3)**, 403–408, https://doi.org/10.1007/s00340-008-3135-y, URL https://doi.org/10.1007/s00340-008-3135-y.

Dauhut, T., J.-P. Chaboureau, P. H. Haynes, and T. P. Lane, 2018: The mechanisms leading to a stratospheric hydration by overshooting convection. *Journal of the Atmospheric Sciences*, **75 (12)**, 4383 – 4398, https://doi.org/10.1175/JAS-D-18-0176.1, URL https://journals.ametsoc.org/view/journals/atsc/75/12/jas-d-18-0176.1.xml.

de F. Forster, P. M., and K. P. Shine, 1999: Stratospheric water vapour changes as a possible contributor to observed stratospheric cooling. *Geophysical Research Letters*, **26 (21)**, 3309–3312, https://doi.org/https://doi.org/10.1029/1999GL010487, URL https://agupubs.onlinelibrary.wiley.com/doi/abs/10.1029/1999GL010487, https://agupubs.onlinelibrary.wiley.com/doi/pdf/10.1029/1999GL010487.

de Reus, M., and Coauthors, 2009: Evidence for ice particles in the tropical stratosphere from in-situ measurements. *Atmospheric Chemistry and Physics*, **9 (18)**, 6775–6792, https://doi.org/10.5194/acp-9-6775-2009, URL https://acp.copernicus.org/articles/9/6775/2009/.

Dessler, A., and Coauthors, 2016: Transport of ice into the stratosphere and the humidification of the stratosphere over the 21st century. *Geophysical Research Letters*, **43 (5)**, 2323–2329, https://doi.org/https://doi.org/10.1002/2016GL067991, URL https://agupubs.onlinelibrary.wiley.com/doi/abs/10.1002/2016GL067991, https://agupubs.onlinelibrary.wiley.com/doi/pdf/10.1002/2016GL067991.

Dessler, A. E., M. R. Schoeberl, T. Wang, S. M. Davis, and K. H. Rosenlof, 2013: Stratospheric water vapor feedback. *Proceedings of the National Academy of Sciences*, **110 (45)**, 18 087–18 091, https://doi.org/10.1073/pnas.1310344110, URL https://www.pnas.org/doi/abs/10.1073/pnas.1310344110, https://www.pnas.org/doi/pdf/10.1073/pnas.1310344110.

Dessler, A. E., and S. C. Sherwood, 2004: Effect of convection on the summertime extratropical lower stratosphere. *Journal of Geophysical Research: Atmospheres*, **109 (D23)**, https://doi.org/https://doi.org/10.1029/2004JD005209, URL https://agupubs.onlinelibrary.wiley.com/doi/abs/10.1029/2004JD005209, https://agupubs.onlinelibrary.wiley.com/doi/pdf/10.1029/2004JD005209.

Dickerson, R. R., and Coauthors, 1987: Thunderstorms: An important mechanism in the transport of air pollutants. *Science*, **235 (4787)**, 460–465, https://doi.org/10.1126/science.235.4787.460, URL https://www.science.org/doi/abs/10.1126/science.235.4787.460, https://www.science.org/doi/pdf/10.1126/science.235.4787.460.

Dobson, G. M. B., 1956: Origin and distribution of the polyatomic molecules in the atmosphere. *Proc. Roy. Soc. London*, **236 (1205)**, 187–193, https://doi.org/10.1098/rspa.1956.0127.

Duncan, B. N., J. A. Logan, I. Bey, I. A. Megretskaia, R. M. Yantosca, P. C. Novelli, N. B. Jones, and C. P. Rinsland, 2007: Global budget of co, 1988–1997: Source estimates and validation with a global model. *Journal of Geophysical Research: Atmospheres*, **112 (D22)**, https://doi.org/https://doi.org/10.1029/2007JD008459, URL https://agupubs.onlinelibrary.wiley.com/doi/abs/10.1029/2007JD008459, https://agupubs.onlinelibrary.wiley.com/doi/pdf/10.1029/2007JD008459.

Fischer, H., and Coauthors, 2003: Deep convective injection of boundary layer air into the lowermost stratosphere at midlatitudes. *Atmospheric Chemistry and Physics*, **3 (3)**, 739–745, https://doi.org/10.5194/acp-3-739-2003, URL https://acp.copernicus.org/articles/3/739/2003/.

Fromm, M. D., and R. Servranckx, 2003: Transport of forest fire smoke above the tropopause by supercell convection. *Geophysical Research Letters*, **30 (10)**, https://doi.org/https://doi.org/10.1029/2002GL016820, URL https://agupubs.onlinelibrary.wiley.com/doi/abs/10.1029/2002GL016820, https://agupubs.onlinelibrary.wiley.com/doi/pdf/10.1029/2002GL016820.

Gordon, A. E., and C. R. Homeyer, 2022: Sensitivities of cross-tropopause transport in midlatitude overshooting convection to the lower stratosphere environment. *Journal of Geophysical Research: Atmospheres*, **127 (13)**, e2022JD036 713, https://doi.org/https://doi.org/10.1029/2022JD036713, URL https://agupubs.onlinelibrary.wiley.com/doi/abs/10.1029/2022JD036713, e2022JD036713 2022JD036713, https://agupubs.onlinelibrary.wiley.com/doi/pdf/10.1029/2022JD036713.

Gordon, A. E., and Coauthors, 2024: Airborne observations of upper troposphere and lower stratosphere composition change in active convection producing above-anvil cirrus plumes. *Atmospheric Chemistry and Physics*, **24 (13)**, 7591–7608, https://doi.org/10.5194/acp-24-7591-2024, URL https://acp.copernicus.org/articles/24/7591/2024/.

Grosvenor, D. P., T. W. Choularton, H. Coe, and G. Held, 2007: A study of the effect of overshooting deep convection on the water content of the ttl and lower stratosphere from cloud resolving model simulations. *Atmospheric Chemistry and Physics*, **7 (18)**, 4977–5002, https://doi.org/10.5194/acp-7-4977-2007, URL https://acp.copernicus.org/articles/7/4977/2007/.

Hanisco, T. F., and Coauthors, 2007: Observations of deep convective influence on stratospheric water vapor and its isotopic composition. *Geophysical Research Letters*, **34 (4)**, https://doi.org/https://doi.org/10.1029/2006GL027899, URL https://agupubs.onlinelibrary.wiley.com/doi/abs/10.1029/2006GL027899, https://agupubs.onlinelibrary.wiley.com/doi/pdf/10.1029/2006GL027899.

Hannun, R. A., A. K. Swanson, S. A. Bailey, T. F. Hanisco, T. P. Bui, I. Bourgeois, J. Peischl, and T. B. Ryerson, 2020: A cavity-enhanced ultraviolet absorption instrument for high-precision, fast-time-response ozone measurements. *Atmospheric Measurement Techniques*, **13 (12)**, 6877–6887, https://doi.org/10.5194/amt-13-6877-2020, URL https://amt.copernicus.org/articles/13/6877/2020/.

Hegglin, M. I., and Coauthors, 2004: Tracing troposphere-to-stratosphere transport above a mid-latitude deep convective system. *Atmospheric Chemistry and Physics*, **4 (3)**, 741–756, https://doi.org/10.5194/acp-4-741-2004, URL https://acp.copernicus.org/articles/4/741/2004/.

Herman, R. L., and Coauthors, 2017: Enhanced stratospheric water vapor over the summertime continental united states and the role of overshooting convection. *Atmospheric Chemistry and Physics*, **17 (9)**, 6113–6124, https://doi.org/10.5194/acp-17-6113-2017, URL https://acp.copernicus.org/articles/17/6113/2017/.

Hersbach, H., and Coauthors, 2020: The era5 global reanalysis. *Quarterly Journal of the Royal Meteorological Society*, **146 (730)**, 1999–2049, https://doi.org/https://doi.org/10.1002/qj.3803, URL https://rmets.onlinelibrary.wiley.com/doi/abs/10.1002/qj.3803, https://rmets.onlinelibrary.wiley.com/doi/pdf/10.1002/qj.3803.

Hoffmann, L., and R. Spang, 2022: An assessment of tropopause characteristics of the era5 and era-interim meteorological reanalyses. *Atmospheric Chemistry and Physics*, **22 (6)**, 4019–4046, https://doi.org/10.5194/acp-22-4019-2022, URL https://acp.copernicus.org/articles/22/4019/2022/.

Holton, J. R., P. H. Haynes, M. E. McIntyre, A. R. Douglass, R. B. Rood, and L. Pfister, 1995: Stratosphere-troposphere exchange. *Reviews of Geophysics*, **33 (4)**, 403–439, https://doi.org/https://doi.org/10.1029/95RG02097, URL https://agupubs.onlinelibrary.wiley.com/doi/abs/10.1029/95RG02097, https://agupubs.onlinelibrary.wiley.com/doi/pdf/10.1029/95RG02097.

Homeyer, C. R., and K. P. Bowman, 2022: Algorithm description document for version 3.1 of the three-dimensional gridded nexrad wsr-88d radar (gridrad) dataset. *University of Oklahoma-Texas A&M University Tech. Rep.*

Homeyer, C. R., J. D. McAuliffe, and K. M. Bedka, 2017: On the development of above-anvil cirrus plumes in extratropical convection. *Journal of the Atmospheric Sciences*, **74 (5)**, 1617 – 1633, https://doi.org/10.1175/JAS-D-16-0269.1, URL https://journals.ametsoc.org/view/journals/atsc/74/5/jas-d-16-0269.1.xml.

Homeyer, C. R., L. L. Pan, and M. C. Barth, 2014a: Transport from convective overshooting of the extratropical tropopause and the role of large-scale lower stratosphere stability. *Journal of Geophysical Research: Atmospheres*, **119 (5)**, 2220–2240, https://doi.org/https://doi.org/10.1002/2013JD020931, URL https://agupubs.onlinelibrary.wiley.com/doi/abs/10.1002/2013JD020931, https://agupubs.onlinelibrary.wiley.com/doi/pdf/10.1002/2013JD020931.

Homeyer, C. R., T. N. Sandmæl, C. K. Potvin, and A. M. Murphy, 2020: Distinguishing characteristics of tornadic and nontornadic supercell storms from composite mean analyses of radar observations. *Monthly Weather Review*, **148 (12)**, 5015 – 5040, https://doi.org/10.1175/MWR-D-20-0136.1, URL https://journals.ametsoc.org/view/journals/mwre/148/12/mwr-d-20-0136.1.xml.

Homeyer, C. R., and Coauthors, 2014b: Convective transport of water vapor into the lower stratosphere observed during double-tropopause events. *Journal of Geophysical Research: Atmospheres*, **119 (18)**, 10,941–10,958, https://doi.org/https://doi.org/10.1002/2014JD021485, URL https://agupubs.onlinelibrary.wiley.com/doi/abs/10.1002/2014JD021485, https://agupubs.onlinelibrary.wiley.com/doi/pdf/10.1002/2014JD021485.

Homeyer, C. R., and Coauthors, 2023: Extreme altitudes of stratospheric hydration by midlatitude convection observed during the dcotss field campaign. *Geophysical Research Letters*, **50 (18)**, e2023GL104 914, https://doi.org/https://doi.org/10.1029/2023GL104914, URL https://agupubs.onlinelibrary.wiley.com/doi/abs/10.1029/2023GL104914, e2023GL104914 2023GL104914, https://agupubs.onlinelibrary.wiley.com/doi/pdf/10.1029/2023GL104914.

Homeyer, C. R., and Coauthors, 2024: Stratospheric hydration processes in tropopause-overshooting convection revealed by tracer-tracer correlations from the dcotss field campaign. *Journal of Geophysical Research: Atmospheres*, **129 (16)**, e2024JD041 340, https://doi.org/https://doi.org/10.1029/2024JD041340, URL https://agupubs.onlinelibrary.wiley.com/doi/abs/10.1029/2024JD041340, e2024JD041340 2024JD041340, https://agupubs.onlinelibrary.wiley.com/doi/pdf/10.1029/2024JD041340.

Hoskins, B. J., 1991: Towards a pv-θ view of the general circulation. *Tellus B*, **43 (4)**, 27–35, https://doi.org/https://doi.org/10.1034/j.1600-0889.1991.t01-3-00005.x, URL https://onlinelibrary.wiley.com/doi/abs/10.1034/j.1600-0889.1991.t01-3-00005.x, https://onlinelibrary.wiley.com/doi/pdf/10.1034/j.1600-0889.1991.t01-3-00005.x.

Houze Jr., R. A., 2004: Mesoscale convective systems. *Reviews of Geophysics*, **42 (4)**, https://doi.org/https://doi.org/10.1029/2004RG000150, URL https://agupubs.

onlinelibrary.wiley.com/doi/abs/10.1029/2004RG000150, https://agupubs.onlinelibrary.wiley.com/doi/pdf/10.1029/2004RG000150.

Jensen, E. J., and Coauthors, 2020: Assessment of observational evidence for direct convective hydration of the lower stratosphere. *Journal of Geophysical Research: Atmospheres*, **125 (15)**, e2020JD032 793, https://doi.org/https://doi.org/10.1029/2020JD032793, URL https://agupubs.onlinelibrary.wiley.com/doi/abs/10.1029/2020JD032793, e2020JD032793 10.1029/2020JD032793, https://agupubs.onlinelibrary.wiley.com/doi/pdf/10.1029/2020JD032793.

Jost, H.-J., and Coauthors, 2004: In-situ observations of mid-latitude forest fire plumes deep in the stratosphere. *Geophysical Research Letters*, **31 (11)**, https://doi.org/https://doi.org/10.1029/2003GL019253, URL https://agupubs.onlinelibrary.wiley.com/doi/abs/10.1029/2003GL019253, https://agupubs.onlinelibrary.wiley.com/doi/pdf/10.1029/2003GL019253.

Khaykin, S., and Coauthors, 2009: Hydration of the lower stratosphere by ice crystal geysers over land convective systems. *Atmospheric Chemistry and Physics*, **9 (6)**, 2275–2287, https://doi.org/10.5194/acp-9-2275-2009, URL https://acp.copernicus.org/articles/9/2275/2009/.

Khaykin, S. M., and Coauthors, 2022: Persistence of moist plumes from overshooting convection in the asian monsoon anticyclone. *Atmospheric Chemistry and Physics*, **22 (5)**, 3169–3189, https://doi.org/10.5194/acp-22-3169-2022, URL https://acp.copernicus.org/articles/22/3169/2022/.

Khordakova, D., C. Rolf, J.-U. Grooß, R. Müller, P. Konopka, A. Wieser, M. Krämer, and M. Riese, 2022: A case study on the impact of severe convective storms on the water vapor mixing ratio in the lower mid-latitude stratosphere observed in 2019 over europe. *Atmospheric Chemistry and Physics*, **22 (2)**, 1059–1079, https://doi.org/10.5194/acp-22-1059-2022, URL https://acp.copernicus.org/articles/22/1059/2022/.

Kley, D., A. L. Schmeltekopf, K. Kelly, R. H. Winkler, T. L. Thompson, and M. McFarland, 1982: Transport of water through the tropical tropopause. *Geophysical Research Letters*, **9 (6)**, 617–620, https://doi.org/https://doi.org/10.1029/GL009i006p00617, URL https://agupubs.onlinelibrary.wiley.com/doi/abs/10.1029/GL009i006p00617, https://agupubs.onlinelibrary.wiley.com/doi/pdf/10.1029/GL009i006p00617.

Le, T. V., and W. A. Gallus Jr., 2012: Effect of an extratropical mesoscale convective system on water vapor transport in the upper troposphere/lower stratosphere: A modeling study. *Journal of Geophysical Research: Atmospheres*, **117 (D3)**, https://doi.org/https://doi.org/10.1029/2011JD016685, URL https://agupubs.onlinelibrary.wiley.com/doi/abs/10.1029/2011JD016685, https://agupubs.onlinelibrary.wiley.com/doi/pdf/10.1029/2011JD016685.

Liu, N., C. Liu, and L. Hayden, 2020: Climatology and detection of overshooting convection from 4 years of gpm precipitation radar and passive microwave observations. *Journal of Geophysical Research: Atmospheres*, **125 (7)**, e2019JD032 003, https://doi.org/https://doi.org/10.1029/2019JD032003, URL https://agupubs.onlinelibrary.wiley.com/doi/abs/10.1029/2019JD032003, e2019JD032003 2019JD032003, https://agupubs.onlinelibrary.wiley.com/doi/pdf/10.1029/2019JD032003.

Meteorology, W., 1957: A three-dimensional science: Second session of the commission for aerology. *WMO bull*, **4 (2)**, 134–138.

Mullendore, G. L., D. R. Durran, and J. R. Holton, 2005: Cross-tropopause tracer transport in midlatitude convection. *Journal of Geophysical Research: Atmospheres*, **110 (D6)**, https://doi.org/https://doi.org/10.1029/2004JD005059, URL https://agupubs.onlinelibrary.wiley.com/doi/abs/10.1029/2004JD005059, https://agupubs.onlinelibrary.wiley.com/doi/pdf/10.1029/2004JD005059.

Mullendore, G. L., A. J. Homann, S. T. Jorgenson, T. J. Lang, and S. A. Tessendorf, 2013: Relationship between level of neutral buoyancy and dual-doppler observed mass detrainment levels in deep convection. *Atmospheric Chemistry and Physics*, **13 (1)**, 181–190, https://doi.org/10.5194/acp-13-181-2013, URL https://acp.copernicus.org/articles/13/181/2013/.

Murillo, E. M., and C. R. Homeyer, 2022: What determines above-anvil cirrus plume infrared temperature? *Journal of the Atmospheric Sciences*, **79 (12)**, 3181 – 3194, https://doi.org/10.1175/JAS-D-22-0080.1, URL https://journals.ametsoc.org/view/journals/atsc/79/12/JAS-D-22-0080.1.xml.

Murphy, A. M., C. R. Homeyer, and K. Q. Allen, 2023: Development and investigation of gridrad-severe, a multiyear severe event radar dataset. *Monthly Weather Review*, **151 (9)**, 2257 – 2277, https://doi.org/10.1175/MWR-D-23-0017.1, URL https://journals.ametsoc.org/view/journals/mwre/151/9/MWR-D-23-0017.1.xml.

NASA/LARC/SD /ASDC, 2022: Dynamics and chemistry of the summer stratosphere radar and satellite (remote sensing) data products. NASA Langley Atmospheric Science Data Center DAAC, URL https://doi.org/10.5067/ASDC/DCOTSS-Radar-Satellite-Data_1.

NASA/LARC/SD/ASDC, 2022: Dynamics and chemistry of the summer stratosphere airborne data products. NASA Langley Atmospheric Science Data Center DAAC, URL https://doi.org/10.5067/ASDC/DCOTSS-Aircraft-Data_1.

O'Neill, M. E., L. Orf, G. M. Heymsfield, and K. Halbert, 2021: Hydraulic jump dynamics above supercell thunderstorms. *Science*, **373 (6560)**, 1248–1251, https://doi.org/10.1126/science.abh3857, URL https://www.science.org/doi/abs/10.1126/science.abh3857, https://www.science.org/doi/pdf/10.1126/science.abh3857.

Pan, L. L., and Coauthors, 2009: Tropospheric intrusions associated with the secondary tropopause. *Journal of Geophysical Research: Atmospheres*, **114 (D10)**, https://doi.org/https://doi.org/10.1029/2008JD011374, URL https://agupubs.onlinelibrary.wiley.com/doi/abs/10.1029/2008JD011374, https://agupubs.onlinelibrary.wiley.com/doi/pdf/10.1029/2008JD011374.

Pan, L. L., and Coauthors, 2014: Thunderstorms enhance tropospheric ozone by wrapping and shedding stratospheric air. *Geophysical Research Letters*, **41 (22)**, 7785–7790, https://doi.org/https://doi.org/10.1002/2014GL061921, URL https://agupubs.onlinelibrary.wiley.com/doi/abs/10.1002/2014GL061921, https://agupubs.onlinelibrary.wiley.com/doi/pdf/10.1002/2014GL061921.

Park, M., W. J. Randel, L. K. Emmons, and N. J. Livesey, 2009: Transport pathways of carbon monoxide in the asian summer monsoon diagnosed from model of ozone and related tracers (mozart). *Journal of Geophysical Research: Atmospheres*, **114 (D8)**, https://doi.org/https://doi.org/10.1029/2008JD010621, URL https://agupubs.onlinelibrary.wiley.com/doi/abs/10.1029/2008JD010621, https://agupubs.onlinelibrary.wiley.com/doi/pdf/10.1029/2008JD010621.

Phoenix, D. B., and C. R. Homeyer, 2021: Simulated impacts of tropopause-overshooting convection on the chemical composition of the upper troposphere and lower stratosphere. *Journal of Geophysical Research: Atmospheres*, **126 (21)**, e2021JD034 568, https://doi.org/https://doi.org/10.1029/2021JD034568, URL https://agupubs.onlinelibrary.wiley.com/doi/abs/10.1029/2021JD034568, e2021JD034568 2021JD034568, https://agupubs.onlinelibrary.wiley.com/doi/pdf/10.1029/2021JD034568.

Poulida, O., R. R. Dickerson, and A. Heymsfield, 1996: Stratosphere-troposphere exchange in a midlatitude mesoscale convective complex: 1. observations. *Journal of Geophysical Research: Atmospheres*, **101 (D3)**, 6823–6836, https://doi.org/https://doi.org/10.1029/95JD03523, URL https://agupubs.onlinelibrary.wiley.com/doi/abs/10.1029/95JD03523, https://agupubs.onlinelibrary.wiley.com/doi/pdf/10.1029/95JD03523.

Randel, W. J., E. Moyer, M. Park, E. Jensen, P. Bernath, K. Walker, and C. Boone, 2012: Global variations of hdo and hdo/h2o ratios in the upper troposphere and lower stratosphere derived from ace-fts satellite measurements. *Journal of Geophysical Research: Atmospheres*, **117 (D6)**, https://doi.org/https://doi.org/10.1029/2011JD016632, URL https://agupubs.onlinelibrary.wiley.com/doi/abs/10.1029/2011JD016632, https://agupubs.onlinelibrary.wiley.com/doi/pdf/10.1029/2011JD016632.

Randel, W. J., M. Park, L. Emmons, D. Kinnison, P. Bernath, K. A. Walker, C. Boone, and H. Pumphrey, 2010: Asian monsoon transport of pollution to the stratosphere. *Science*, **328 (5978)**, 611–613, https://doi.org/10.1126/science.1182274, URL https://www.science.org/doi/abs/10.1126/science.1182274, https://www.science.org/doi/pdf/10.1126/science.1182274.

Ray, E. A., and Coauthors, 2004: Evidence of the effect of summertime midlatitude convection on the subtropical lower stratosphere from crystal-face tracer measurements. *Journal of Geophysical Research: Atmospheres*, **109 (D18)**, https://doi.org/https://doi.org/10.1029/2004JD004655, URL https://agupubs.onlinelibrary.wiley.com/doi/abs/10.1029/2004JD004655, https://agupubs.onlinelibrary.wiley.com/doi/pdf/10.1029/2004JD004655.

Romps, D. M., and Z. Kuang, 2009: Overshooting convection in tropical cyclones. *Geophysical Research Letters*, **36 (9)**, https://doi.org/https://doi.org/10.1029/2009GL037396, URL https://agupubs.onlinelibrary.wiley.com/doi/abs/10.1029/2009GL037396, https://agupubs.onlinelibrary.wiley.com/doi/pdf/10.1029/2009GL037396.

Sargent, M. R., and Coauthors, 2013: A new direct absorption tunable diode laser spectrometer for high precision measurement of water vapor in the upper troposphere and lower stratosphere. *Review of Scientific Instruments*, **84 (7)**, 074 102, https://doi.org/10.1063/1.4815828, URL https://doi.org/10.1063/1.4815828, https://pubs.aip.org/aip/rsi/article-pdf/doi/10.1063/1.4815828/13518038/074102_1_online.pdf.

Sayres, D. S., J. B. Smith, D. M. Wilmouth, A. Pandey, C. R. Homeyer, K. P. Bowman, and J. G. Anderson, 2024: Using the nama as a natural integrator to quantify the convective contribution to lower stratospheric water vapor over north america. *Journal of Geophysical Research: Atmospheres*, **129 (17)**, e2024JD041 641, https://doi.org/https://doi.org/10.1029/2024JD041641, URL https://agupubs.onlinelibrary.wiley.com/doi/abs/10.1029/2024JD041641, e2024JD041641 2024JD041641, https://agupubs.onlinelibrary.wiley.com/doi/pdf/10.1029/2024JD041641.

Schwartz, M. J., W. G. Read, M. L. Santee, N. J. Livesey, L. Froidevaux, A. Lambert, and G. L. Manney, 2013: Convectively injected water vapor in the north american summer lowermost stratosphere. *Geophysical Research Letters*, **40 (10)**, 2316–2321, https://doi.org/https://doi.org/10.1002/grl.50421, URL https://agupubs.onlinelibrary.wiley.com/doi/abs/10.1002/grl.50421, https://agupubs.onlinelibrary.wiley.com/doi/pdf/10.1002/grl.50421.

Scott, S. G., T. P. Bui, K. R. Chan, and S. W. Bowen, 1990: The meteorological measurement system on the nasa er-2 aircraft. *Journal of Atmospheric and Oceanic Technology*, **7 (4)**, 525 – 540, https://doi.org/10.1175/1520-0426(1990)007⟨0525:TMMSOT⟩2.0.CO;2, URL https://journals.ametsoc.org/view/journals/atot/7/4/1520-0426_1990_007_0525_tmmsot_2_0_co_2.xml.

Setvák, M., and Coauthors, 2010: Satellite-observed cold-ring-shaped features atop deep convective clouds. *Atmospheric Research*, **97 (1)**, 80–96, https://doi.org/https://doi.org/10.1016/j.atmosres.2010.03.009, URL https://www.sciencedirect.com/science/article/pii/S016980951000058X.

Smith, J. B., and Coauthors, 2017: A case study of convectively sourced water vapor observed in the overworld stratosphere over the united states. *Journal* *of Geophysical Research: Atmospheres*, **122 (17)**, 9529–9554, https://doi.org/https://doi.org/10.1002/2017JD026831, URL https://agupubs.onlinelibrary.wiley.com/doi/abs/10.1002/2017JD026831, https://agupubs.onlinelibrary.wiley.com/doi/pdf/10.1002/2017JD026831.

Solomon, D. L., K. P. Bowman, and C. R. Homeyer, 2016: Tropopause-penetrating convection from three-dimensional gridded nexrad data. *Journal of Applied Meteorology and Climatology*, **55 (2)**, 465 – 478, https://doi.org/10.1175/JAMC-D-15-0190.1, URL https://journals.ametsoc.org/view/journals/apme/55/2/jamc-d-15-0190.1.xml.

Solomon, S., K. H. Rosenlof, R. W. Portmann, J. S. Daniel, S. M. Davis, T. J. Sanford, and G.-K. Plattner, 2010: Contributions of stratospheric water vapor to decadal changes in the rate of global warming. *Science*, **327 (5970)**, 1219–1223, https://doi.org/10.1126/science.1182488, URL https://www.science.org/doi/abs/10.1126/science.1182488, https://www.science.org/doi/pdf/10.1126/science.1182488.

Sprenger, M., M. C. Maspoli, and H. Wernli, 2003: Tropopause folds and cross-tropopause exchange: A global investigation based upon ECMWF analyses for the time period March 2000 to February 2001. *J. Geophys. Res.*, **108 (D12)**, 8518, https://doi.org/10.1029/2002JD002587.

Stohl, A., 2001: A 1-year lagrangian "climatology" of airstreams in the northern hemisphere troposphere and lowermost stratosphere. *Journal of Geophysical Research: Atmospheres*, **106 (D7)**, 7263–7279, https://doi.org/https://doi.org/10.1029/2000JD900570, URL https://agupubs.onlinelibrary.wiley.com/doi/abs/10.1029/2000JD900570, https://agupubs.onlinelibrary.wiley.com/doi/pdf/10.1029/2000JD900570.

Stohl, A., and Coauthors, 2003: Stratosphere-troposphere exchange: A review, and what we have learned from staccato. *Journal of Geophysical Research: Atmospheres*, **108 (D12)**, https://doi.org/https://doi.org/10.1029/2002JD002490, URL https://agupubs.onlinelibrary.wiley.com/doi/abs/10.1029/2002JD002490, https://agupubs.onlinelibrary.wiley.com/doi/pdf/10.1029/2002JD002490.

Tang, Q., M. J. Prather, and J. Hsu, 2011: Stratosphere-troposphere exchange ozone flux related to deep convection. *Geophysical Research Letters*, **38 (3)**, https://doi.org/https://doi.org/10.1029/2010GL046039, URL https://agupubs.onlinelibrary.wiley.com/doi/abs/10.1029/2010GL046039, https://agupubs.onlinelibrary.wiley.com/doi/pdf/10.1029/2010GL046039.

Tinney, E. N., and C. R. Homeyer, 2021: A 13-year trajectory-based analysis of convection-driven changes in upper troposphere lower stratosphere composition over the united states. *Journal of Geophysical Research: Atmospheres*, **126 (3)**, e2020JD033 657, https://doi.org/https://doi.org/10.1029/2020JD033657, URL https://agupubs.onlinelibrary.wiley.com/doi/abs/10.1029/2020JD033657, e2020JD033657 2020JD033657, https://agupubs.onlinelibrary.wiley.com/doi/pdf/10.1029/2020JD033657.

Tinney, E. N., C. R. Homeyer, K. M. Bedka, and B. R. Scarino, 2024: The response of tropopause-overshooting convection over north america to climate change. *Journal of Climate*, **37 (23)**, 6183 – 6200, https://doi.org/10.1175/JCLI-D-23-0745.1, URL https://journals.ametsoc.org/view/journals/clim/37/23/JCLI-D-23-0745.1.xml.

Tinney, E. N., C. R. Homeyer, L. Elizalde, D. F. Hurst, A. M. Thompson, R. M. Stauffer, H. Vömel, and H. B. Selkirk, 2022: A modern approach to a stability-based definition of the tropopause. *Monthly Weather Review*, **150 (12)**, 3151 – 3174, https://doi.org/10.1175/MWR-D-22-0174.1, URL https://journals.ametsoc.org/view/journals/mwre/150/12/MWR-D-22-0174.1.xml.

Toon, O. B., and Coauthors, 2016: Planning, implementation, and scientific goals of the studies of emissions and atmospheric composition, clouds and climate coupling by regional surveys (seac4rs) field mission. *Journal of Geophysical Research: Atmospheres*, **121 (9)**, 4967–5009, https://doi.org/https://doi.org/10.1002/2015JD024297, URL https://agupubs.onlinelibrary.wiley.com/doi/abs/10.1002/2015JD024297, https://agupubs.onlinelibrary.wiley.com/doi/pdf/10.1002/2015JD024297.

Venkat Ratnam, M., S. Ravindra Babu, S. S. Das, G. Basha, B. V. Krishnamurthy, and B. Venkateswararao, 2016: Effect of tropical cyclones on the stratosphere–troposphere exchange observed using satellite observations over the north indian ocean. *Atmospheric Chemistry and Physics*, **16 (13)**, 8581–8591, https://doi.org/10.5194/acp-16-8581-2016, URL https://acp.copernicus.org/articles/16/8581/2016/.

Wang, P. K., 2003: Moisture plumes above thunderstorm anvils and their contributions to cross-tropopause transport of water vapor in midlatitudes. *Journal of Geophysical Research: Atmospheres*, **108 (D6)**, https://doi.org/https://doi.org/10.1029/2002JD002581, URL https://agupubs.onlinelibrary.wiley.com/doi/abs/10.1029/2002JD002581, https://agupubs.onlinelibrary.wiley.com/doi/pdf/10.1029/2002JD002581.

Wang, P. K., S. H. Su, Z. Charvát, J. Šťástka, and H. Lin, 2011: Cross tropopause transport of water by mid-latitude deep convective storms: A review. *Terrestrial, Atmospheric, and Oceanic Sciences*, **22 (5)**, 447–462, https://doi.org/0.3319/TAO.2011.06.13.01(A), URL http://tao.cgu.org.tw/index.php/articles/archive/atmospheric-science/item/1028-2011061301a.

Weinstock, E. M., and Coauthors, 1994: New fast response photofragment fluorescence hygrometer for use on the nasa er-2 and the perseus remotely piloted aircraft. *Review of Scientific Instruments*, **65 (11)**, 3544–3554, https://doi.org/10.1063/1.1144536, URL https://doi.org/10.1063/1.1144536, https://pubs.aip.org/aip/rsi/article-pdf/65/11/3544/19076629/3544_1_online.pdf.

Weinstock, E. M., and Coauthors, 2007: Quantifying the impact of the north american monsoon and deep midlatitude convection on the subtropical lowermost stratosphere using in situ measurements. *J. Geophys. Res.*, **112 (D18310)**, https://doi.org/10.1029/2007JD008554.

Wernli, H., and M. Bourqui, 2002: A lagrangian “1-year climatology” of (deep) cross-tropopause exchange in the extratropical northern hemisphere. *Journal of Geophysical Research: Atmospheres*, **107 (D2)**, ACL 13–1–ACL 13–16, https://doi.org/https://doi.org/10.1029/2001JD000812, URL https://agupubs.onlinelibrary.wiley.com/doi/abs/10.1029/2001JD000812, https://agupubs.onlinelibrary.wiley.com/doi/pdf/10.1029/2001JD000812.

Zhan, R., and Y. Wang, 2012: Contribution of tropical cyclones to stratosphere-troposphere exchange over the northwest pacific: Estimation based on airs satellite retrievals and era-interim data. *Journal of Geophysical Research: Atmospheres*, **117 (D12)**, https://doi.org/https://doi.org/10.1029/2012JD017494, URL https://agupubs.onlinelibrary.wiley.com/doi/abs/10.1029/2012JD017494, https://agupubs.onlinelibrary.wiley.com/doi/pdf/10.1029/2012JD017494.